UNIVERSITÀ
DEGLI STUDI
DI PADOVA

Head Office: Università degli Studi di Padova

DEPARTMENT: Salute della Donna e del Bambino

Ph.D. COURSE: Medicina dello Sviluppo e Scienze della Programmazione Sanitaria
CURRICULUM: Emato-oncologia, Genetica, Malattie rare e Medicina predittiva
SERIES Ciclo 34°

PEDIATRIC AND FETAL GASTROINTESTINAL ORGANOIDS: THREE-DIMENSIONAL CULTURES FOR *IN VITRO* DISEASE MODELLING

Coordinator: Prof. Gianni Bisogno
Supervisor: Prof Piergiorgio Gamba

Ph.D. student : Elisa Zambaiti

PhD student
Dr. Elisa Zambaiti

ABSTRACT

Aim

Adult COVID-19 is mainly respiratory illness, but in children GI symptoms are more frequent. Furthermore, fetuses are rarely affected by COVID-19. Organoids are a relatively new tool to in vitro establish long-living culture that three-dimensionally resemble the tissue of origin and may both maintain the stemness and fully differentiate in all cell types.

As a proof of concept, we aimed to develop a culture system for gastrointestinal organoids (GIOs) to investigate SARS-CoV-2 infection in gastric epithelium across the lifespan.

Methods

GIO were derived from 8-21 week fetuses and from pediatric and adult tissues. They were cultured using chemically-defined medium, to test their ability to maintain stemness and to fully differentiate. GIO were analyzed in correlation to the surrounding ECM.

Reverse cellular polarity Organoids (RP-GOs) were induced and incubated with SARS-CoV-2. All experiments were analyzed by qPCR, immunofluorescence and qualitative analysis as appropriate.

Results

Gastrointestinal organoids can be isolated from all gestational ages, demonstrating normal gastric epithelial morphology and expressing mature gastric cell types including, the niche, secretive, and enteroendocrine cells. These cultures may be maintained indefinitely *in vitro* and cultured in GMP-compliant conditions. RP-GOs exhibit apical-out polarity, exposing ACE2 on the external surface, optimizing conditions for viral infection. Viral nucleoprotein was demonstrated in cells undergoing apoptosis, with pediatric RP-GOs most susceptible and efficiently infected compared to fetal and adult organoids.

PhD student
Dr. Elisa Zambaiti

Conclusions

We have successfully established an efficient gastrointestinal organoid culture systems for all ages, from fetal life to adulthood. Organoid-based technology can be used for *in vitro* disease modelling, drug testing or cell therapy. The application of GMP compliant rules makes the clinical translation closer.

INTRODUCTION

Recently, the development of organoids from adult stem cells and from human pluripotent stem cells, allowed the formation of an organ *in vitro* that histologically and functionally resembles their tissue of origin. The establishment of an in vitro three-dimensional gastrointestinal organ model has required a deep understanding of the mechanisms underlying cell homeostasis and the spatial-temporal cell specification throughout organ morphogenesis in this tissue.

We will first describe the possibility to efficiently derive organoids from fetal, pediatric and adult tissues and prove their ability to maintain their stemness throughout the unlimited expansion, and functionally differentiate to mature phenotypes.

We then studied the interaction between the organoids and the surrounding extracellular matrix and generated an extracellular matrix completely compatible with GMP guidelines that could potentially be useful for the clinical translation.

Due to their unique characteristics, organoids are a promising cell source for tissue regeneration, tissue repair, and could be applied as a therapeutic tool for various disease models. As a proof of concept, we finally infected the organoids with SARS-CoV2 to test their ability to *in vitro* model the mechanisms of infection and postulate possible transmission pathways.

BACKGROUND

Epithelium composition: focus on gastrointestinal tract

Different types of epithelia cover the body surface and some internal organs, such as the digestive system, protecting us from various pathogens assaults, tissue damage or dysregulated immune response. During lifetimes, digestive epithelia are constantly exposed to acute and chronic insults which finally cause these tissues to be in frequent regeneration processes [1]. The need to constantly self-renew and to differentiate into specialized cell types, that give each tissue its specific function, involves the maintenance of a proper balance between cell proliferation and death among the various cell types that compose the epithelium in a process called homeostasis. Stem cells are the principal actors of this process and their presence reside in a complex microenvironment called niche, composed of diverse cell types of which some are responsible to maintain the local environment and other to imprint the differentiation toward other cell types, depending on the tissue of origin [2]. Epithelial–mesenchymal crosstalk involves Fibroblast Growth Factor (FGF), wingless (WNT) and CDX signaling and it is crucial in both morphogenesis and homeostasis. Therefore, if the crosstalk between niche cells, surrounding mesenchyme and more differentiated epithelial cells is perturbed, it may result in the loss of the epithelial functions or in an anomalous crypt-villus units' formation.

The intestine provides an excellent system to study both tissue morphogenesis and homeostatic regulation because most lineages have well-defined spatial and temporal succession [3]. Epithelial lineages derive from a common embryonic endodermal progenitor cell [4] and subsequently differentiate in transient amplifying (TA) cells, localized at the base of the intestinal crypt together with the stem cells (marked with Leucine-Rich containing G protein-coupled receptor, LGR5) and producing mature absorptive enterocytes, which make up the vast majority of the intestinal epithelial cells and secretory cells such as goblet, Paneth and enteroendocrine cells [5]. The development of the crypt-villus unit relies on the different distribution of local signals, with WNT, R-spondin and Epidermal Growth Factor (EGF) signaling at the bottom of the crypt to

maintain the niche and promote cell replication and Bone Morphogenic Protein (BMP) signaling at the top of the villus to promote cell differentiation [6, 7]. The spatiotemporal distribution of these signaling pathways derives from the defined role of mesenchymal cells surrounding the intestine and the establishment of the stem cell niche from development through adulthood is dependent on the epithelial–mesenchymal crosstalk.

The stomach can be anatomically divided into the fundus, corpus and the antrum, which opens into the duodenum. Each of these parts is lined by a glandular epithelium, except in rodents which have a large forestomach lined with simple columnar epithelium. Glands begin as polyclonal structures in the embryo but become a monoclonal unit in the adult stomach [8]. The glands can be divided into the luminal pit region, the isthmus, the neck and the base. The intestinal stem cell marker LGR5 can be found at the bottom of stomach glands. Lineage tracing experiments proved that these cells could generate entire glands in the antrum/pyloric region [9]. Besides this region, a second region of stem cell activity has been identified in the stomach. The isthmus shows a high cellular turnover and it is the location of a population of mostly quiescent stem cells activated if needed. Upon epithelial injury the stem cell population actively contributes to gland regeneration, thus acting as a reserve stem cell population. Daughter cells of the isthmus stem cell population are thought to migrate bidirectionally to the top and the bottom of the gland [10]. It is yet to clarify by which mechanisms the isthmus and gland bottom stem cells compete in the homeostasis and regeneration of the glands. Like in the intestinal epithelium, mesenchymal signaling is involved in the maintenance of gastric homeostasis.

Similarly to the intestine, five distinct cell types differentiate from gastric stem cells: foveolar (pit) cells, located at the top of stomach glands and producing mucus, shows a turn over every 3 days; zymogenic (chief) cells at the bottom of the glands secrete digestive enzymes such as pepsinogen and turn over every few months; abundant parietal (oxyntic) cells along the gland shaft secrete HCl; rare endocrine cells (accounting for <2% of the epithelium), secrete hormones; and finally rare tuft cells, which express chemosensory markers and characteristic apical microtubules. Each of these cell types may be generated by stem and progenitor cells located either in the isthmus of gland units or at the bottom of it which alternatively activate during life-long self-renewal.

Fever data exists instead on the development of the gastric epithelium across different embryonic stages. The understanding of the physiological changes during morphogenesis

and periodic renewal on the different types of epithelia is crucial to investigate the mechanism of *in vitro* culture systems.

Gastrointestinal Organoids: applying theorical knowledge to the dish

Organoids are 3D structures capable to reproduce *in vitro* the complex structure of the tissue of origin while also maintaining the stemness crucial to self-renew, to say it in other words, they constitute artificial mini-organs *in vitro*.
Organoids may be created either isolating stem cells from a tissue or driving pluripotent stem cells to a specific lineage. Stem cells are combined with proper biological factors to reproduce in culture the *in vivo* niche components, necessary for stemness maintenance.
By doing so, the organoids recapitulate in vivo epithelial structures: intestinal single stem cells (ISCs), for instance, initially form villus-like cystic structures with a single central lumen and subsequently the cyst projects crypt-like budding structures outward. Eventually mini-gut organoids form multiple-budding organoid structures containing Lgr5+ stem cells and all types of differentiated cells. Interestingly, the localization of each cell type in organoids reflects the localization *in vivo*: ISCs and Paneth cells are localized at the bottom of budding structures, whereas mature enterocytes migrate to the central cyst structure (Figure I).

In vivo the main actors in stemness maintenance are Wnt3 secreted by Paneth cells [11], and R-spondin 2/3 being produced by the intestinal stroma [12]. *In vitro*, R-spondin1 needs to be supplemented constantly as a substitute for the missing stroma. When Wnt is supplemented to the medium of Lgr5+ cells, they rapidly grow and form cystic structures solely composed of stem and progenitor cells, whereas Wnt3a can be omitted from the medium once Paneth cells are present. The Wnt gradient along the crypt-villus axis is very important for cellular differentiation and it peaks at the crypt bottom where the Lgr5+ stem cell/Paneth cell membranes form a pool for secreted Wnt [13].
The complex BMP/TGF-β signaling pathway, also originating from the mesenchyme, is related to cell differentiation and, in culture, it is responsible for the long-term cultivation efficiency of the cells: depletion of BMP antagonists, like Noggin, reduce cellular proliferation [14]. Despite being important in cancer-associated proliferation, low doses

of TGF-β kinase/activin receptor-like kinase inhibitors, such as A83–01, are required for long term organoid cultures [15].

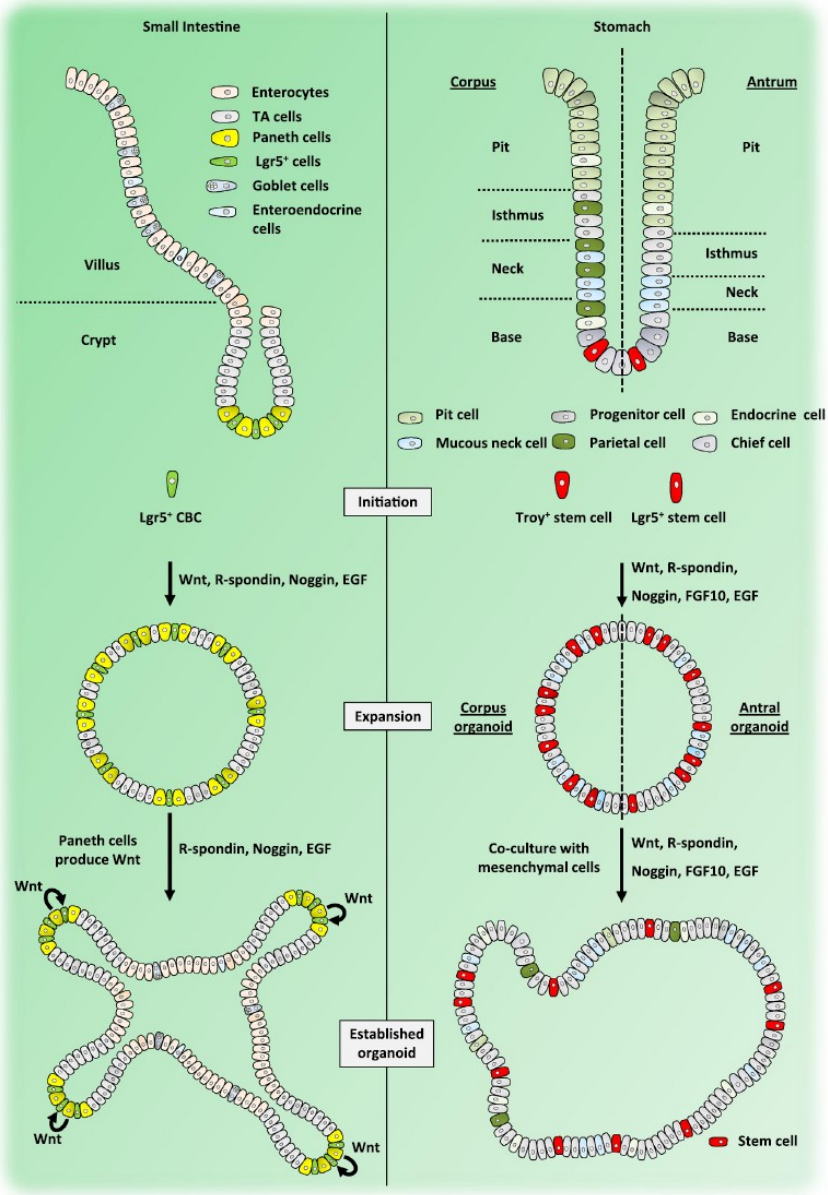

Figure I. From Merker et al [16]. Architecture and differentiation conditions for intestinal and gastric organoids compared to the structure of the intestinal and gastric units.

In addition to Wnt and BMP/TGF-β signaling several other pathways are important in the creation of the niche *in vitro*. Similarly to BMP, EGF signaling (produced by Paneth cells in the niche) is required for long-term organoid expansion [17]. Intestinal stem cells

divide symmetrically, but their fate is determined by contact or loss of contact to Paneth cells, which therefore constitute a key regulatory element within the niche. As in the *in vivo* situation, Notch signaling from stem cells maintain the contact with the Wnt secreting Paneth cells and, whenever lost, drive the differentiation toward secretory goblet cells [18]; on the contrary, cells under p38 inhibition fails to differentiate toward secretor lineages.
A number of supplements further helps increasing the efficiency of organoid culture initiation and propagation, such as for instance B27 (increases sphere-forming efficiency) and N-acetylcysteine (an antioxidant direct towards ROS and mucolytic).

To summarize the abovementioned pathways, in an exemplary list that does not want to be exhaustive, stem cell self-renewal in mini-gut organoids is primarily controlled by extrinsic niche factors and thus the culture employs unique serum-free and mesenchymal-free growth environments comprising the defined niche factors Wnt3a, R-Spondin (interacts with Wnt), Noggin (inhibits BMP signaling), A83-01 (Transforming Growth Factor TGFb inhibitor), SB202190 (MAPK inhibitor, p38 inhibitor), growth factors (EGF, FGF), N2 supplement (human insulin, human transferrin, sodium selenite, putrescine, and progesterone), N-Acetyl Cysteine, gastrin (stimulates acid secretion and the cellular renewal of the epithelium) and the Rock inhibitor Y-27632 (to help recovering of the cells after their isolation).

Since 2009, when the first a mini-gut culture system was established for mouse intestinal LGR5+ stem cells by Sato et al [11], the optimal composition of many niche factors has been tailored according to the type and origin of cells. Mouse small intestinal organoids can be cultured with essential niche factors (EGF, Noggin, and R-spondin), whereas additional niche factors are required for other tissue stem cells. Mouse colon organoids require Wnt-3A, and human intestinal and colonic organoids further require p38 inhibitor and TGF-β inhibitor [11]. Alternatively, human colonic organoids can be cultured under the presence of Wnt-3A, prostaglandin E2, and nicotinamide in addition to mouse small intestinal organoid culture conditions [19].

Similarly, gastric organoids had been first established from LGR5+ stomach adult stem cells [20], and later on from pluripotent stem cells [21]. The development of stomach organoids was facilitated by the existing knowledge on Intestinal organoids and many of

the component were directly transferred to that new culture type. This was extremely helpful, as the gastric stem cell niche composition and behavior are much less well defined as compared to the intestine. Using a modification of the culture condition developed for the intestine, organoids from the Lgr5 stem cells in the gland bottom and stem cells from the isthmus [22] were easily isolated and characterized. These organoids contain all cell types normally found in the tissue, i.e., endocrine cells, parietal cells, chief cells, mucous gland neck cells and surface mucous pit cells. Many of the cell types are nowadays fully differentiated in culture in gastric organoids, except parietal cell, indicating that certain components are still missing in the culture medium. As a further proof of that, the co-culture with mesenchymal cells allow differentiation in all subtypes [23], highlighting the important of the epithelial-mesenchymal crosstalk also in the stomach. Additional components to the intestinal organoid culture are the growth factor FGF10 (necessary for gland formation and proliferation [24]) and the peptide hormone gastrin.

11

Steps for *in vivo* application

As further mentioned elsewhere, organoids may be useful for clinical translation. However, few studies have reported the investigation of human organoids for in vivo applications. Moreover, to apply these culture systems in a clinical environment, various limitations must be overcome. In particular, one constraint relates to the ability to expand these organoids in conditions that are GMP-compliant. This concept relates to the fact that every step of the manufacturing and production process of a potential therapy should undergo a set of guidelines, standards and regulations published by health authorities to ensure consistent and closely controlled products that are safer for patients.
In the context of organoids and their possible translation to the *in vivo* biological use, this applies to all steps from isolation from tissue to *in vitro* cell expansion and experimentation. As most of the factor needed for organoids cultured are already produced in GMP compliant manner, a crucial aspect to be investigated is the use of

As intimate attachment between the epithelium and basal membrane is essential for epithelial cell survival through integrin signaling, most organoids are generated by the

simple expansion of stem cells in 3D hydrogel systems, consisting of highly hydrated polymer networks, and are commonly cultured on those 3D structures of extracellular matrix (ECM)-derived proteins. Mouse tumor matrices with poorly defined environmental signaling, such as Engelbreth-Holm-Swarm (EHS) sarcoma, have often been used for organoid expansion in vitro. Matrigel is composed of ECM molecules, such as laminin, collagen type IV, entactin, and heparan sulfate proteoglycans, as well as some growth factors, such as TGF-β and FGF. Intestinal organoids can be maintained in pure collagen type I gel for a long time, but the culture efficiency is lower than that of organoids maintained in Matrigel, suggesting that intestinal epithelium favors the ECM molecules in the latter [25].

Attempts to produce artificial matrices that could overcome these limitations for clinical translation have so far shown encouraging results in mouse [26] and, recently, in human organoids [27]. However, it is a real challenge to define all the relevant information necessary to instruct specific tissue remodeling and regeneration. This is also related to the partial information in the literature about the biochemical signature of tissue-specific ECM [28, 29]. As a consequence, synthetic matrices can only partially reproduce some of the native ECM features which commonly include adhesion signals and proteo-cleavable structures.

The use of naturally derived materials from decellularized tissues (DT) could be compatible for clinical translation while enhancing the presence of ECM components and thus finally allowing normal cell culture. Indeed, DT have been already used clinically, for example as cardiac valve substitutions and for the patch repair of large surgical defects [30, 31]. Additionally, cell-laden DT efficiently promote in vivo tissue regeneration as demonstrated both by preclinical data and experimental human transplantation. These processes suggest that ECM not only provides a structural support, but also delivers biochemical signals that are fundamental to assisting the regeneration process [32]. These environmental cues are not limited to ECM tissue-specific proteins, but also include soluble factors absorbed within the ECM protein network. Hydrogels derived from DT potentially have the advantage of providing the cells with all the information they need for their growth and expansion, while also being GMP-compliant [33]. ECM-derived hydrogels could be also used in the future for organoid transplantation supporting in vivo organoids growth and bioprinting in clinically relevant environments [34].

In the Results session we will demonstrate the creation of an ECM-derived gel that allow the complex culture of organoids, offering a bridge toward their possible use in clinical setting.

Gastrointestinal organoids for disease modelling

The utilization of organoids derived from both adult stem cells and human pluripotent stem cells offers new opportunities to understand epithelial homeostasis and physiopathological processes [35].

Being able to maintain the mesenchymal niche cells and all epithelial cell types (such as tuft cells or enteroendocrine cells) in the intestinal organoid is crucial to studying disease states, such as inflammatory bowel disease [36]. Moreover, organoids recapitulate different absorptive and digestive functions determined by the proximal-distal intestinal axis [37]. Organoid-based models of inflammatory bowel disease have been established from the inflamed mucosa of patients [38], and their characterization reproduce the typical changes seen in the clinical scenario, with an epithelial alteration due to inflammatory features, pseudo-stratification, slow growth, altered polarization and decreased expression of tight-junction proteins. Similarly, *Helicobacter pylori* infection in gastric organoids may be easily achieved by microinjection into the lumen of the organoids [39], and they may reproduce important hallmarks of the infection to study mechanisms of gastric carcinoma initiation and progression [40].

In pediatrics, organoids have been so far used as an in vitro model of different pathologies. One example is necrotizing enterocolitis [41], in which GI organoids injured in culture express pro-inflammatory cytokines [42]. Moreover, human intestinal organoids from ileum of preterm infant who underwent surgery for necrotizing enterocolitis stricture in the absence of ileum inflammation were successfully isolated and used for drug testing [43].

Another filed of interest is the treatment of Hirschsprung's disganglionosis, for which complex cultures with epithelial component together with the functional enteric nervous system (ENCC) have been studied [44]. After stimulating ENCCs-containing GI organoids in electrical-field stimulation, these organoids could regulate waves of

propagating contraction, which indicates that the neuromuscular components had been well-formed. Enteric nervous system function has also been successfully restored in tissue-engineered small intestine derived from human intestinal organoids. ENCC organoids were transplanted together with the organoids on scaffolds and sutured into mice omentum and formed submucosal and myenteric ganglions [45].
In addition, intestinal organoids are robust tools for studying genetic diseases due to their stability. Surprisingly, cystic transmembrane conductance regulator (CFTR) gene mutation in the intestinal organoids derived from patients with cystic fibrosis might be corrected by the CRISPR/Cas9 genomic editing system. These genomic edited organoids are able to restore CFTR function, opening the possibility of future gene therapy [46].
Short bowel syndrome is the main cause of intestinal failure in children [47]; its treatment goals include to promote intestinal adaptation and increase intestinal absorption, providing the possibility of gaining enteral autonomy and discontinuation of parenteral nutrition. Development of intestinal organoids potentially creates a novel way of experimentally investigating and treating short bowel syndrome by direct infusion within pre-existing intestine (i.e. the colon) ore by creating in vitro organs to be transplanted (i.e. scaffolds loaded with organoids).

Usefulness of organoids as an *in vitro* model of infection: SARS-CoV2

Reliable *in vitro* models capable of reproducing complex *in vivo* systems are becoming increasingly important also in life sciences and play a crucial role in the investigation of emerging pathogens like Severe Acute Respiratory Syndrome CoronaVirus 2 (SARS-CoV-2). In the context of the COronaVIrus Disease 2019 (COVID-19) pandemic, it is still unclear how gastrointestinal virus replication might affect the clinical outcome of infection, the development of immunity and the dynamic transmission in the population. While it has been shown that SARS-CoV-2 is frequently detected in rectal samples of affected children and adults [48, 49], it remains to be determined whether the virus is able to produce a primary infection throughout the entire GI tract, or if its presence could be related in part to a passive transport of contaminated sputum coming from the upper respiratory tract. Moreover, the ability of SARS-CoV-2 to persist in the GI tract after

respiratory clearance, has not yet been fully elucidated in terms of viral infectivity, possibly impairing important public health and policy measures for the control of the disease.

These concerns are particularly relevant in children who appear on average to suffer a less severe respiratory illness compared to adults, despite recording more prominent GI symptoms [50], or acting as relatively asymptomatic carriers of the virus. Moreover, although vertical transmission of SARS-CoV-2 seems to be anecdotal, it is still unclear if this lack of infection relates to the inability of the virus to migrate through the placenta [51], to the low susceptibility of the fetal cells to infection, or simply on low viremic loads.

MATERIALS AND METHODS

Human tissue isolation and cell culture

Human tissue samples

Tissues were collected at Great Ormond Street Hospital, London, UK. Human fetal stomachs were dissected from tissue obtained immediately after termination of pregnancy from 8 to 21 PCW (post conception week), in compliance with the bioethics legislation in the UK. Fetal samples were sourced via the Joint MRC/Wellcome Trust Human Developmental Biology Resource under informed ethical consent with Research Tissue Bank ethical approval (08/H0712/34+5 and 08/H0906/21+5).

Isolation of fetal human gastric stem cells and organoids creation (GO)

Biopsies from human fetal tissue abovementioned were isolate and processed as follows. Stomach biopsies were collected in ice-cold sterile phosphate buffered solution (PBS – Sigma-Aldrich) and processed within a few hours of collection. Gastric crypt stem cells were isolated from specimens following well-established dissociation protocols [52, 53]. Briefly, fetal stomachs were cut open longitudinally along the lesser curvature. Specimens were cold-washed in a plate with chelating buffer (sterile Milli-Q water (Merck Millipore) with 5.6 mmol/L Na2HPO4, 8.0 mmol/L KH2PO4, 96.2 mmol/L NaCl, 1.6 mmol/L KCl, 43.4 mmol/L sucrose, 54.9 mmol/L D- sorbitol, 0 390 .5 mmol/L DL-dithiothreitol, pH 7, all from Sigma-Aldrich). Mucus was removed with a glass coverslip and mucosa was stripped from muscle layer. Tissue was cut in small pieces, transferred in a 15 mL tube in new chelating buffer and pipetted repeatedly. Supernatant was discarded and 10 mL of 10 mM ethylenediaminetetraacetic acid (EDTA) was added and incubated for 10 min at room temperature. EDTA was discarded and mucosa pieces were washed in ice cold PBS with Ca2+/Mg2+ (Sigma-Aldrich). Tissue was transferred to a new 10 cm plate on ice and pressure was applied on top with a sterile 3.5 cm plate, to release the crypts from the mucosa. Crypts were collected in ice-cold ADMEM+++ (Advanced DMEM/F-12, Dulbecco's Modified Eagle Medium/Ham's F-12), composed

of Advanced DMEM F-12, 10 mM HEPES (4-(2-hydroxyethyl)-1-piperazineethanesulfonic acid), 2 mM Glutamax (substitute for L-glutamine), 1% Penicillin/Streptomycin (all from Thermo Fisher Scientific). Medium with glands was filtered through a 40 μm strainer and centrifuged at 300 g for 5 min at 4°C. Supernatant was discarded and ice cold liquid Matrigel® Basement Membrane Matrix Growth Factor Reduced (GFR) (Corning 354230) was added to the pellet and thoroughly resuspended. Droplets of 30 μL were aliquoted on warmed multi-well plates and incubated for 20 min at 37°C for gelation. Medium was added and changed every 3 days. For medium recipes refer to Table I.

With this method, we derived a biobank of 5 early fetal lines (from Carnegie Stage CS23 to PCW 11), 6 late fetal lines (from PCW 18 to PCW 21).

Table I. Human gastric organoid medium

Component	**Final conc.**
Advanced DMEM F-12 (Thermo 12634)	To volume
HEPES (Thermo 15630080)	10 mM
Glutamax (Thermo 35050061)	2 mM
B-27 supplement minus vitamin A (Thermo 12587010)	1 X
n-acetylcysteine (Sigma A9165)	1.25 mM
Pen/Strep (Thermo 15140122)	1 %
Wnt-3A (Peprotech 315-20)	100 ng/mL
R-spondin 1 (Peprotech 120-38)	500 ng/mL
Noggin (R&D 6057-NG)	100 ng/mL
EGF (Thermo PMG8043)	50 ng/mL
Gastrin (Sigma G9020)	10 nM
FGF10 (Peprotech)	50 ng/ml
TGFb inhibitor (A83-01) (Sigma SML0788)	500 nM

Human fetal small intestinal organoids (SIO) isolation and culture

Small intestines (SIs) were dissected from human fetal tissue fragments obtained immediately after termination of pregnancy a mentioned above. The obtained tissue was washed through once with ice-cold PBS, cleared of any mesenteric or fatty tissue and cut longitudinally. Following a further series of PBS washes, a cover slip was used to shave away the villi and the remaining tissue was cut into 2–3 mm pieces and washed

vigorously. This was then incubated in 2 mM EDTA in PBS for 30 min followed by vigorous shaking for 5 min in PBS. The obtained supernatant, containing the intestinal crypts, was centrifuged at 800 rpm for 5 min at 4 °C (Hettich zentrifugen Rotina 420). The pellet was washed once with basal media (Advanced DMEM/F12 media, supplemented with 1% of each GlutaMAX, HEPES and Penicillin/Streptomycin) and centrifuged at 1000 rpm. The pellet was re-suspended in Matrigel growth factor reduced and plated onto a 24-well plate. Primocin 1× (Thermo Fisher) and ROCK (Rho Kinase) inhibitor 10 μm are added after isolation. For medium recipe look in Table II.

Table ll. Human small intestinal organoid medium

Component	**Final conc.**
Advanced DMEM F-12 (Thermo 12634)	To volume
HEPES (Thermo 15630080)	10 mM
Glutamax (Thermo 35050061)	2 mM
B-27 supplement minus vitamin A (Thermo 12587010)	1 X
n-acetylcysteine (Sigma A9165)	1.25 mM
Pen/Strep (Thermo 15140122)	1 %
Wnt-3A (Peprotech 315-20)	100 ng/mL
R-spondin 1 (Peprotech 120-38)	500 ng/mL
Noggin (R&D 6057-NG)	100 ng/mL
EGF (Thermo PMG8043)	50 ng/mL
Gastrin (Sigma G9020)	10 nM
GSK-3 inhibitor (CHIR 99021) (Tocris 4423)	3 μM
TGFb inhibitor (A83-01) (Sigma SML0788)	500 nM
P38 inhibitor (SB202190) (Sigma S7067)	10 μM
Prostaglandin E2 (Cambridge cay14010)	10 nM

Culture of pediatric intestinal and gastric human organoids.

Human pediatric SI and stomach samples of ≅ 0.5 cm2 where processed as they were obtained. SI crypt stem cells and gastric crypt stem cells were isolated from pediatric biopsies following well-established dissociation protocols [54, 55]. Isolated crypts at first passage (p0) were cultured in Matrigel growth factor reduced droplets, or in 4 mg/mL ECM gel. For the experiments, a total of 4 pediatric lines (from 4 months to 11 years-old) were established. For media recipes look in Table I and II.

Culture of adult intestinal and gastric human organoids.

Adult organoids, used as control in the SARS-CoV2 experiments, were derived in the Hubrecht Institute (Netherlands) following surgical research license, derived from biopsied of two different patients aged 45 and 71 years.

Passage of organoids in ECM gel and Matrigel.

Cell were passaged every 6–8 days depending on the growth of each line as follows. To passage the organoids, ECM gel and Matrigel droplets were thoroughly disrupted by pipetting in the well and transferred to tubes in ice. ECM removal could be aided with 20 min treatment of the droplets with Cell Recovery Solution (Corning) at 4 °C. Cells were washed with 10 mL of cold basal DMEM F-12 +++ (F-12 + P/S + HEPES + Glutamax) and spin at 200 × g at 4 °C. Supernatant was discarded. If any ECM or Matrigel was left, wash was repeated. The pellet was resuspended in 1mL of cold basal medium and organoids were manually disrupted by narrow (flamed) glass pipette pre-wet in BSA 1% in PBS, to avoid adhesion to the glass. Cells were washed, pelleted and supernatant was discarded. Almost-dry pellets of disaggregated organoids were thoroughly resuspended either in cold liquid Matrigel or in cold ECM equilibrated gel, aliquoted in 30–40 µL droplets in Petri dishes and incubated at 37 °C for 30 min to form a gel. For single cell colony formation, organoids pellets were treated with TrypLE Express for 5–7 min (depending on organoid size and type) at 37 °C and accurate pipetting. Disaggregated cells were washed, pelleted, and resuspended in culture medium with ROCK inhibitor.

Polarity reversion (RP-GO)

Fully grown gastric organoids at day 7 after single cell disaggregation were removed from surrounding extracellular matrix using a modified published protocol [56]. Matrigel was dissolved with 60 min treatment of the droplets with Cell Recovery Solution (Corning) at 4°C. Organoids were retrieved from the plates using 1% Bovine Serum Albumine (BSA)-coated cut-end tips and transferred to 1% BSA-coated 15 mL tubes. Cells were extensively washed with ice-cold PBS and centrifuged at 200 g for 5 min at 4°C. Supernatant was discarded, the pellet was resuspended in complete medium and transferred to non-tissue culture treated low-adhesive multiwell plates (pre-coated in 1%

BSA). Organoids were cultured in suspension for 3 days to allow reversion of polarity, before use in SARS-CoV2 infection experiments.
Polarity reversion in differentiation medium was created with the basal medium, withdrawing Wnt-3A and CHIR 99021. The RP-GOs differentiated were infected in differentiation medium.

Investigating the correlation between organoid and ECM

Creation of ECM hydrogel mixtures

To investigate the influence of the environment surrounding the organoids on their development, we used a technology developed at VIMM (Veneto Institute of Molecular Medicine, Padova, Italy; under patent evaluation, provisional number 102020000008779) which consists of 3D bioprinting, i.e. the creation of three-dimensional objects in a pre-existing matrix. Using this technology, two different three-dimensional printing models were created with Matrigel/HCC (7-hydroxycoumarin-3-carboxylated) and Matrigel/PEG (HCC-8-arm-polyethylene glycol) mixtures. In both cases the powders of the two compounds (HCC and PEG) were dissolved in PBS: the PEG at a concentration of 300 mg/ml under stirring at room temperature, while the HCC at 100 mg/ml stirring for 10 minutes at 60°. For the culture these dilutions were mixed 50:50 with Matrigel. The crosslink was the achieved by two-photon photo-crosslink, obtained with a Scientific 2-Photon microscope, with specific conditions reported in the published paper [61]. For the purposes of this work, the interesting features of the two blends are that while HCC gelatin provides biochemical signals to organoids, which can adhere to them during growth, PEG gelatin has cell-repellent properties.

Creation of an idrogel GMP compliant

Porcine intestinal tissue collection

Porcine (Sus scrofa domesticus) SI mucosal/submucosal layers from the ‘Pietrain’ breed were used. Piglets up to 3 kg in weight were euthanized via blunt trauma once the criteria outlined by the JSR veterinary advisors (UK) had been met. Once sacrificed, the animals were transported to the lab via courier and the intestine was harvested immediately on arrival (within 6 h of euthanasia). The whole SI was harvested (duodenum, jejunum, and

ileum) and the internal tube was pulled out leaving behind the external layer and mesentery. The retrieved mucosal/submucosal tissue was then extensively cleaned with pressurized water, opened longitudinally, cut into 5 cm pieces and placed in Milli-Q® (Merck Millipore) water overnight at 4°C, on a laboratory rotator, to begin the first step of decellularization. Each batch of ECM was composed of three pooled piglets SI.

Decellularization of the intestinal tissue

The detergent enzymatic treatment (DET) for decellularization, previously established on rat small bowel, was optimized for the porcine intestine [57]. See Figure II below for the images of the main steps of the protocol.

After the first overnight wash, the tissue was decellularized with 4% sodium deoxycholate (Sigma Aldrich) for 4 h at room temperature (RT). This was followed by a washing step in Milli-Q water for 24 h at RT, with multiple water changes throughout, and then a step of 2000kU DNase-I (Sigma Aldrich) in 1M NaCl (Sigma Aldrich) for 3 h at RT. The tissue was then placed in Milli-Q water and washed for 2 days, with multiple water changes. Wash steps are fundamental to remove any cytotoxic residual of sodium deoxycholate. A laboratory rotator was used throughout the decellularization process.

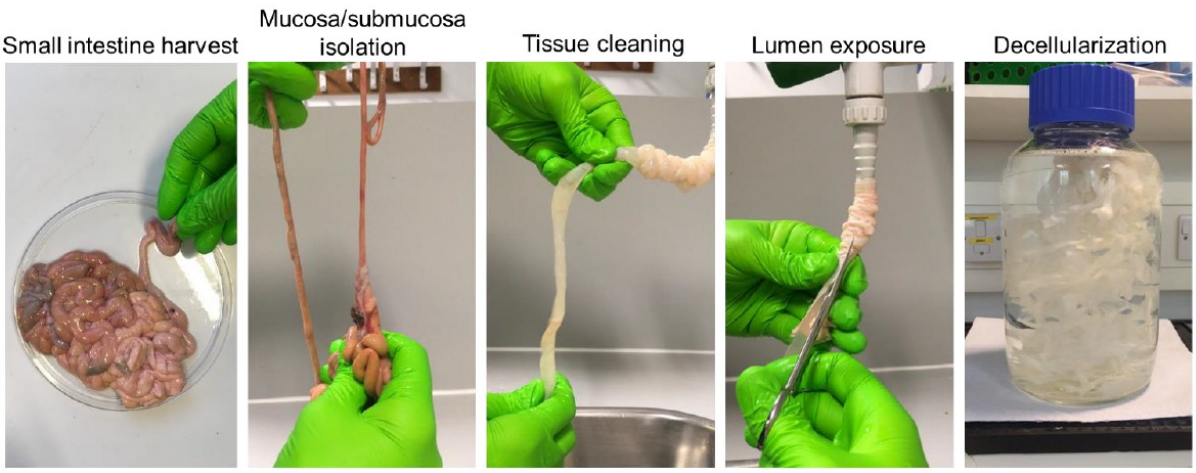

Figure II. Images of the laboratory procedure for piglet small intestine mucosa/submucosa decellularization.

Gelation protocol and cell inclusion

The decellularized porcine intestine was freeze dried for 72 h (Labconco FreeZone Triad Freeze Dry Systems), milled into a thin powder using a mini-mill (Thomas Wiley, mesh 40), sterilized by gamma irradiation (17 kGy for 10 h) and stored at −20 °C until further use. For gelation, the ECM powder was digested at 4, 6, 8, 10 mg/ml in pepsin/HCl solution (1 mg/ml in 0.1M HCl) at RT for 72 h, in constant rotation. Pre-gel was then centrifuged (200–400 g for 5 min) to precipitate and discard eventual undigested particles. Acidic pre-gel solution was commonly used freshly prepared, but it could be stored at 4 °C up to 1 month, or frozen in aliquots at −20 °C for prolonged storage. For cell seeding, while working on ice and immediately prior to use, pre-gel solution was equilibrated to cytocompatible salinity adding 10% 10X PBS for mechanical tests, or 10× DMEM F/12 (Thermo Fisher) for cell culture and neutralized to physiological pH of 7.5 by addition of NaOH 10M and thoroughly mixing, with modification of published protocols [58, 59]. During these steps, cut-end pipette tips are used, to facilitate dense gel pipetting. Gel was mixed with cell pellets and aliquot in 30–40 μL droplets in Petri dish. Gelation took place in 30 min in the incubator. Organoids were cultured in 4–6 mg/mL ECM gels. Every batch of intestinal ECM powder had to be carefully tested for biological variability. Digestion potential, deoxycholate residual from bad decellularization washes, gel formation capacity, and suitability to host an organoid culture had to be tested for every new batch before proceeding to experiments. Tissue samples were taken at random immediately post-harvesting and after each cycle of decellularization.

DNA and ECM quantification.

Tissue samples were taken at random immediately post-harvesting or after decellularization protocol for DNA and ECM components quantification. DNA was quantified using a PureLink Genomic DNA Mini Kit (Thermo Fisher). The final concentration of DNA in the samples was measured using a NanoDrop (model NanoDrop 1000 Spectrophotometer by Thermo Fisher). ECM components were quantified using a QuickZyme Collagen assay kit (QuickZyme Biosciences) to measure the collagen, a Blyscan Sulfated Glycosaminoglycan Assay kit (Biocolor) for the glycosaminoglycans (GAGs) and a Fastin Elastin Assay kit (Biocolor) for elastin, according to manufacturers' instructions.

Scanning electron microscopy (SEM).

SEM-images of the cross-section, top and bottom surfaces of the ECM gel were taken to examine surface-topography of the material. All samples were fixed in 2.5% glutaraldehyde (Sigma Aldrich) washed in 0.1M phosphate buffer (pH 7.4), post fixed with 1% OsO4 (osmium tetraoxide)/1.5% Potassium Ferrocyanide K4[Fe(CN)6] in 0.1M phosphate buffer followed by a dH2O wash. Specimens were then dehydrated in a graded ethanol-water series to 100% ethanol (50, 60, 70, 80, 90, 95, and 100%) and critical point-dried using CO2 [60]. The samples were mounted onto aluminum stubs using sticky carbon tabs, oriented so the surfaces of interest were presented to the beam. Samples were coated with a 2 nm-thin layer of Au/Pd using a Gatan ion-beam coater, and viewed using a Jeol 7401 FEG-SEM.

SARS-CoV2 infection

Infection of organoids in suspension

All experiments were conducted between VIMM (Veneto Institute of Molecular Medicine, Padova, Italy) and the Laboratory of Experimental Animal Models (Division of Comparative Biomedical Sciences, Istituto Zooprofilattico Sperimentale delle Venezie, Legnaro, Italy). Intact organoids were embedded in two 3 µl droplets of Matrigel per well, in 24-well plates. Embedded organoids were washed once in DMEM and infected at a MOI (Multiplicity of Infection) of 0.5 by incubation with 250 µl of an expansion medium viral suspension for 2 hours. After removal of the inoculum, organoids were washed twice with a DMEM solution and 400 µl of complete medium were added to each well to maintain the culture at 37 °C with 5% CO2. Differentiated and undifferentiated RP-GOs were infected at MOI of 0.5, 5, and 10 by incubation with 250 µl of an expansion medium viral suspension for 2 hours. After infection, organoids were washed twice in DMEM to remove unbound virus. RP-GOs were dispersed in a 400 µl expansion medium at 37 °C with 5% CO2. For all organoid cultures 50 µl of supernatant were harvested at 0, 24, 48, and 72 hours post infection. An equal volume of expansion medium replaced the sampled supernatant at each collection time. An extra sample at 96 hours post infection was collected for the RP-GOs. Samples were stored at -80°C before titration through the focus forming assay (FFA).

Quantification of stem cell colonies and organoid diameters.

To quantify the colony formation in ECM gels and Matrigel, n ≥ 10 fields of view at 5× per replicate were acquired at the Zeiss Axio Observer A1 and counted. For organoid dimension quantification, n ≥ 50 full grown organoids were randomly quantified in different 5× fields of view per replicate. For a better approximation, 3 diameters per organoid were measured and mean diameter was considered in the final calculation.

Cell viability assay.

Cells were passaged to ECM gel and Matrigel and seeded. Enteroids were expanded for 2 days and tested for combined gel cytocompatibility. Viability assay was performed using Live/Dead™ Viability/Cytotoxicity Kit, for mammalian cells (Thermo Fisher), following supplier instructions. Briefly, organoids were washed with basal DMEM F-12 and incubated in basal medium with Hoechst, calcein-AM and ethidium homodimer-1 for 45 min. Cells in ECM gel and Matrigel droplets were washed twice and analyzed. Hepatocyte organoids vitality was analyzed through Cell Titer-Glo viability assay (Promega) following manufacturer's instructions.

General protocols

Tissue histology

For paraffin embedded sections, samples were fixed in 4% paraformaldehyde solution in PBS for 24 h at RT, washed in dH2O, dehydrated in graded alcohol, embedded and cut into 5 μm sections. For frozen sections, samples were snap frozen in liquid nitrogen, placed in OCT and cut into 7 μm sections. For ECM gel and Matrigel® Basement Membrane Matrix Growth Factor Reduced (GFR) (Corning 354230), droplets were fixed in glutaraldehyde 2% for 2 h. After fixing, another PBS wash was followed with 100–150 μL of 2% agarose solution until the droplet was fully covered. The agarose was removed, taking with it the gel droplet and stored in 70% ethanol. The agarose/hydrogel samples were then dehydrated with a series of ethanol washes with increasing concentrations followed by two xylene washes. Samples were embedded in paraffin and cut into 7 μm sections. Tissue slides were stained according to manufacturers' instructions with Hematoxylin and Eosin (H&E) (Thermo Fisher) and Hoechst 33342 (Thermo Fisher) to

determine the presence of nuclei and Picrosirius Red (PR), Elastic Van Gieson (EVG) and Alcian Blue (AB) (Thermo Fisher) to assess retention of collagen, elastin and glycosaminoglycans respectively.

Immunofluorescences.

Human gastric tissues were fixed in 4% paraformaldehyde (PFA – Sigma-Aldrich) for 2 hours and embedded in paraffin wax, then cut at 7 μm on a microtome. Hematoxylin and Eosin (H&E) tissue slides were stained according to manufacturer's instructions with Hematoxylin and Eosin (H&E) (Thermo Fisher).

Cultured organoids were removed from Matrigel with 30 min treatment of the droplets with Cell Recovery Solution at 4°C. RP-GOs were fixed in suspension by transferring them to 1% BSA pre-coated 1.5 mL tubes, centrifuging and resuspension in 4% PFA for 20 min in rotation. PFA was discarded and quenched with 0.1M NH4Cl for 1 h in rotation. Matrigel droplets (3 μL on glass slides) with embedded organoids were fixed in 2% PFA for 20 min at RT, and then washed.

Immunostaining was performed by blocking and permeabilizing the tissue slides with PBS + Triton X-100 0.1% with BSA 0.5%. Organoid whole-mounts were blocked and permeabilized with PBS + Triton X-100 0.5% with BSA 1% for 2 h at room temperature in rotation. Primary antibodies were incubated in blocking buffer for 24h at 4°C in rotation and extensively washed in PBS + Triton X-100 0.1%. Secondary antibodies were incubated overnight at 4°C in rotation and extensively washed. Slides were mounted in mounting medium, while floating organoids were moved to a glass-bottomed Petri dish and blocked with a coverslip on top. The full list of primary and secondary antibodies is presented in Table III.

Table III. Antibody and molecule list

Antibody/conjugated molecule	**Dilution**
Ezrin (Thermo PA5-29358)	1:100
E-cadherin (BD 610182)	1:100
Ki-67 (ABCAM Ab15580)	1:200
Lysozyme (Genetex GTX72913)	1:100

Olfactomedin-4 (Cell signaling 14369S)	1:50
Cytokeratin-20 (Proteintech 60183-1-lg)	1:100
Zonula occludens-1 (Invitrogen 40-2200)	1:200
Mucin-5AC (Thermo MA5-12178)	1:100
Goat anti-Rabbit 594 (Thermo A11012)	1:500
Goat anti-Rabbit 568 (Thermo A11011)	1:500
Goat anti-Rabbit 488 (Thermo A11008)	1:500
Goat anti-Mouse 488 (Thermo A11001)	1:500
Goat anti-Mouse 568 (Thermo A10037)	1:500
Donkey anti-Goat 647 (Thermo A-21447)	1:500
Anti-Guinea pig (Jackson 706-165-148)	1:500
Anti-Hamster (Abcam AB175716)	1:500
Hoechst 33342 (Thermo H1399)	10 µg/mL
Calcein-AM (Thermo L3224)	3 µM
Ethidium homodimer-1 (Thermo L3224)	3 µM

Image acquisition

Organoids were imaged using a Zeiss Axio Observer A1. Stained sections were acquired on a Leica DMIL microscope and DFC420C camera or using a Hamamatsu Photonics NanoZoomer. Immunofluorescence images of whole mount stainings and sections were acquired on a confocal microscope Zeiss LSM 710.

RESULTS

Defined stages are present during early and late human gastric development

Organoids are organized three dimensional structures that can be grown from stem cells found in adult and fetal tissues. In order to derive a novel *in vitro* gastric model of fetal origin, the tissues isolated from human fetuses were firstly characterized and compared to gastric mucosa obtained from pediatric patients undergoing surgery. Developing stomach structures are shown in Figure III from Carnegie stage (CS) 23 (corresponding to mid-week 8) to post conception week (PCW) 21.

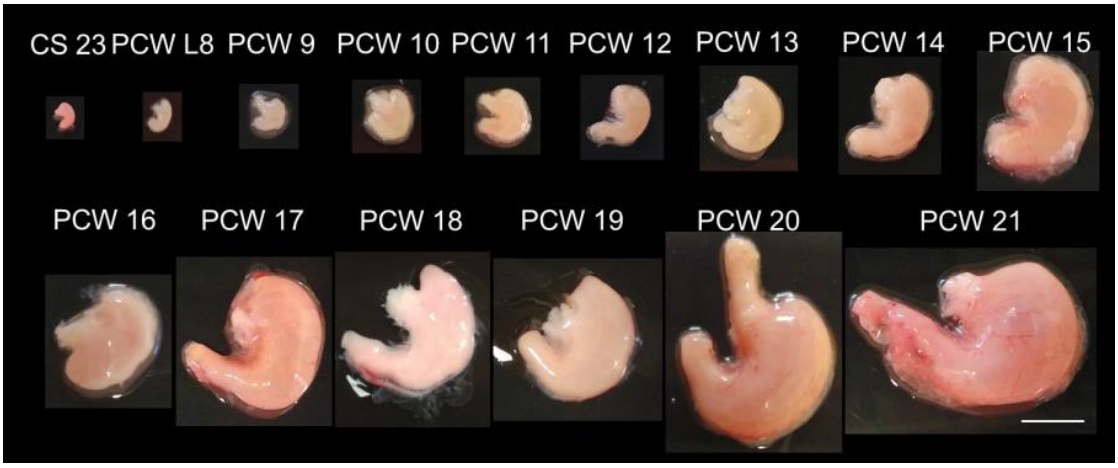

Figure III. Isolated human whole stomachs from terminated pregnancies, from Carnegie stage 23 (mid-week 8) to post conception week (PCW) 21. Scale bar 1 cm.

Gastric crypts start to invaginate between PCW 11 and PCW 12 and form a clearly defined crypt at around PCW 20 (Figure IV).

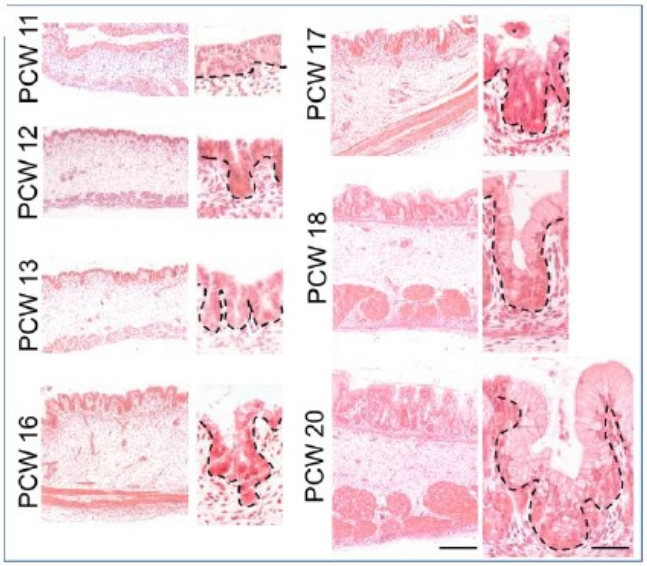

Figure IV. Hematoxylin and Eosin staining of paraffin-embedded stomach sections from PCW 11 to PCW 20. Scale bars 100 µm in lower magnification (left) and 20 µm in higher crypt magnification (right).

We also characterized the appearance of gastric markers during stomach development. Mucin 5AC positive pit mucous cells were evident at PCW 11, while pepsinogen C (marking chief cells) started to emerge at around PCW 20 (Figure III, left). Mucin 6, a gland mucous cell marker, was constitutively expressed from early week 8 (CS 20), together with enteroendocrine cells marked by chromogranin A that were present from mid-week 8 (CS 23) (Figure V, right).

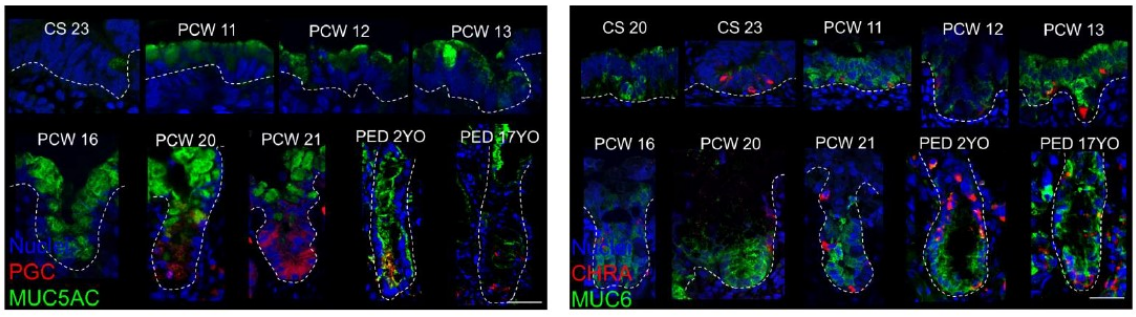

Figure V. (Left) Immunofluorescence panel showing mucin 5AC (MUC5AC) in green, pepsinogen C (PGC) in red and nuclei in blue (Hoechst). Scale bar 20 µm. (Right) Immunofluorescence panel showing mucin 6 (MUC6) in green, chromogranin A (CHRA) in red and nuclei in blue (Hoechst). Scale bar 20 µm.

We then defined three distinct groups of gastric epithelial tissues based on gland maturity: 1) early fetal stomachs from PCW 8 to PCW 15; 2) late fetal stomachs from PCW 17 to PCW 21; 3) pediatric stomachs. Real time quantitative PCR (qPCR) was performed on gastric tissues obtained from these three groups to examine the gene expression changes of stem cell and mature cell markers. A significant correlation between developmental stage and mRNA expression was observed for *AXIN2*, mucin 5AC (*MUC5AC*), pepsinogen A5 (*PGA5*), with a similar trend for chromogranin A (*CHGA*) and ATPase H+/K+ transporting subunit beta (*ATP4B*). On the other hand, expression of leucine rich repeat-containing G-protein coupled receptor 5 (*LGR5*) and somatostatin (*SST*) were significantly higher in the late fetal stomachs.

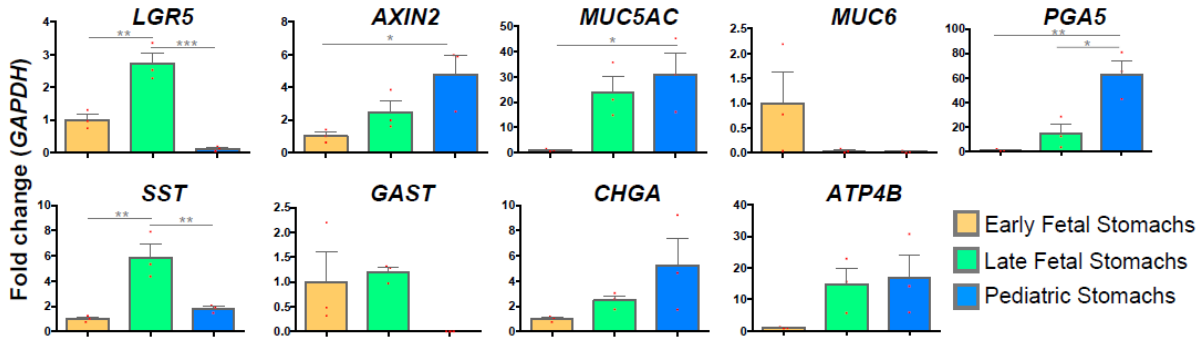

*Figure VI. Real Time PCR analysis of early fetal, late fetal and pediatric stomachs. Relative fold change to GAPDH. Mean ± SEM (n=3). Red dots on the bar charts represent single 625 biological replicates. Ordinary one-way ANOVA; p-value *<0.05, **<0.01, ***<0.001.*

Gastric organoids can be derived from human tissue across different developmental stages

Following gastric tissue characterization, we efficiently extracted glandular crypts from stomach biopsies utilizing chelating buffers and mechanical stress as highlighted in the methods. Adult organoid lines were already available in the laboratory; therefore, we optimized the protocol for novel organoids of fetal and pediatric origin. To improve compatibility with subsequent clinical application of this organoid system, isolated cells were expanded in a chemically defined medium, without the use of animal serum or

conditioned media. Each gastric cytokine, based on previous work [20, 52] was screened and selectively removed from the organoids split to single cells and grown for 10 days to allow clonal organoid formation. While R-spondin 1, wnt-3A and noggin withdrawal led to more unhealthy organoids at day 10, CHIR99021 (GSK-3 inhibitor) proved to be essential in the formation of fetal gastric organoids starting from single cells (Figure VII). No medium-related difference was observed among multiple organoid stages.

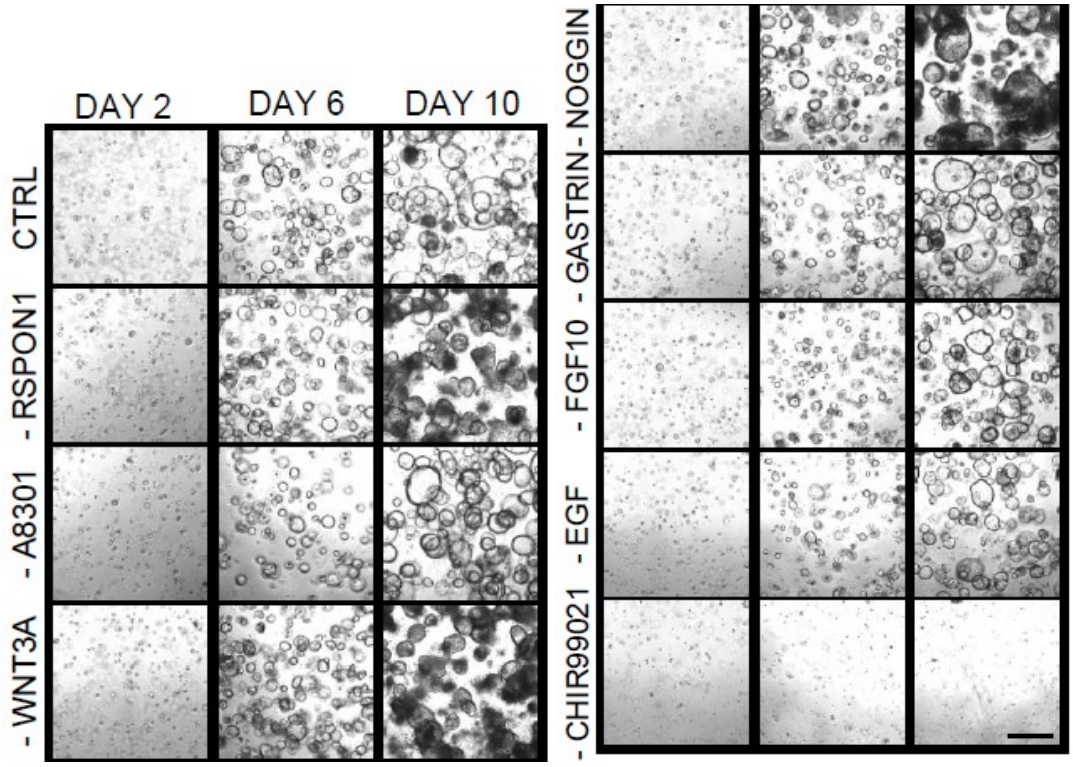

Figure VII. Selective withdrawal of gastric organoid cytokines from control (CTRL) complete medium, in CS 23 (mid-week 8) organoid line split at single cells at passage 7. Scale bar 400 μm.

We then performed isolation of several gastric organoid lines (Figure VI, left). The isolation protocol proved to be highly efficient, and we obtained a biobank composed of multiple developmental stages. These organoids were expanded and counted for several months, showing higher rate of expansion for earlier fetal stages. No plateau was reached in any of the curves even after several months, showing the possibility to obtain stable gastric organoid lines of fetal origin (Figure VIII, right).

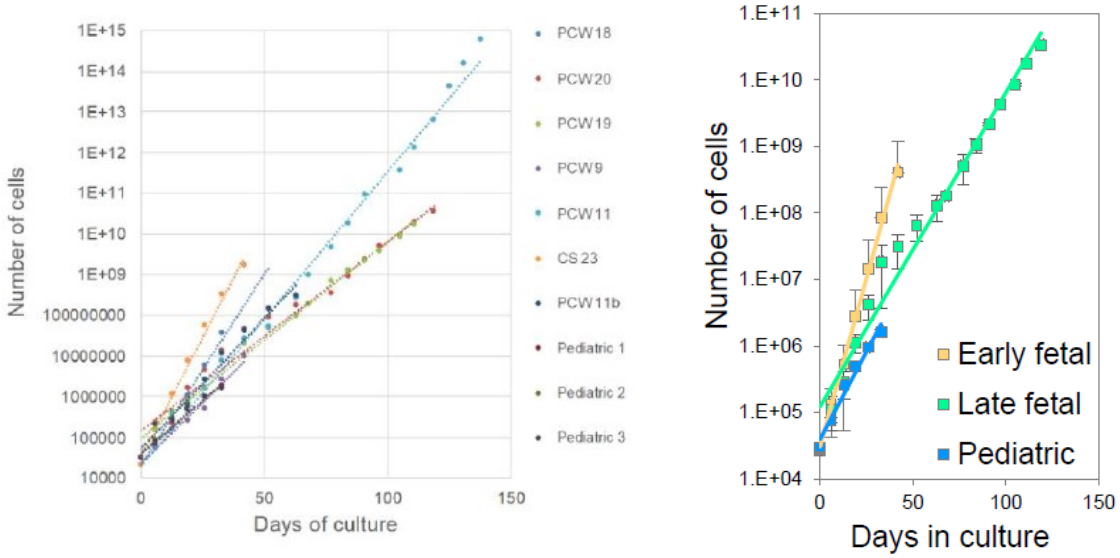

Figure VIII. Cumulative cell counts during days of culture. (Left) all cell lines isolated. (Right) pooled in three main timepoints. Mean ± SD (n=4 biological replicates for early and late fetal, n=3 for pediatric organoids).

Expanding organoids were stained for the epithelial marker ezrin (EZR) and luminal polarized f-actin. MUC5AC was present on the luminal side of the organoids of all stages, with a relatively lower expression in the early PCW 11 (Figure IX).

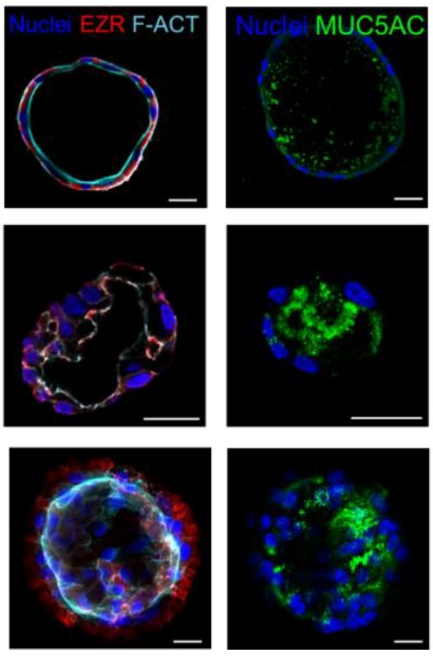

Figure IX. Immunofluorescence panel showing ezrin (EZR) in red, f-actin (F-ACT) in cyan, mucin 5AC (MUC5AC) in green and nuclei in blue (Hoechst). Scale bars 25 µm

After weekly passaging for more than 10 weeks, we further characterized the organoid lines to evaluate genomic stability. Single nucleotide polymorphism arrays on early fetal, late fetal and pediatric organoids showed no chromosomal duplications, no large deletions, nor other karyotype aberrations, demonstrating the organoids are genetically stable after prolonged *in vitro* culture [81].

Real time PCR was performed on organoids grouped in early fetal (CS 23 to PCW 11), late fetal (PCW 18 to PCW 20) and pediatric. Stem cell crypt markers *LGR5* and *AXIN2* were expressed in these organoids, indicating the presence of proliferating cells. *MUC5AC, MUC6, SST* and *AXIN2* showed comparable pattern of expression between stomachs and organoids. On the other hand, *LGR5, PGA5, GAST* and *CHGA* showed a different pattern of expression, while transcript expression of proton pump transporter *ATP4B*, responsible for gastric acid secretion, was lost in the organoid model (Figure X).

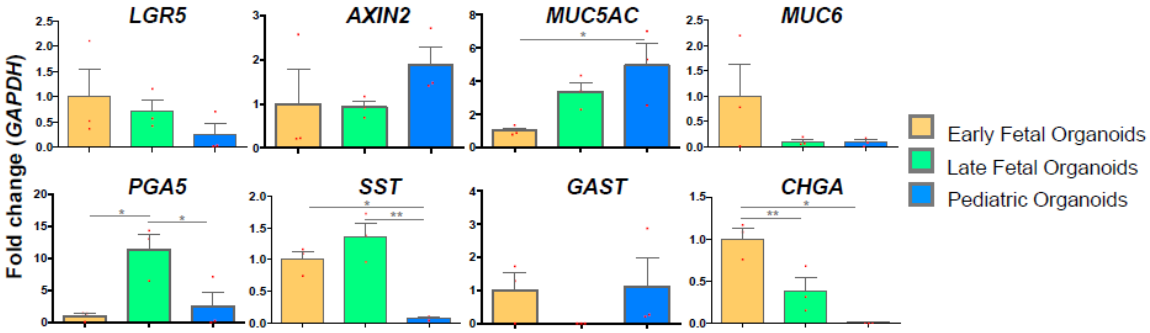

*Figure X. Real Time PCR analysis of early fetal, late fetal and pediatric gastric organoids. Relative fold change to GAPDH. Mean ± SEM (n=3). Red dots on the bar charts represent single biological replicates. Ordinary one-way ANOVA; p-value *<0.05, **<0.01.*

In vitro bioprinting into pre-existing human organoid 3D culture.

Once different cell lines have been proficiently established we aimed to investigate the behavior of the GI organoids related with the ECM. We designed few experiment in which me aimed to build structures surrounding the organoids and analyzed any morphological change. To do so, we applied 3D bioprinting technology to GI organoids culture [61] testing the possibility of fabricating 3D-hydrogel objects in a pre-existing 3D matrix.

We first tested the bio-compatibility of the structures with the organoid culture. We used a 50:50 HCC–gelatin:Matrigel mixture (v/v) to crosslink HCC–gelatin 3D structures of defined position and orientation within the gel. HCC–gelatin–Matrigel 3D gels were able to support the viability and growth of human small intestinal organoids (SIOs) while preserving the possibility of fabricating crosslinked objects within the gel. We fabricated 3D parallelepipeds that were accurately positioned and oriented relative to selected SIOs within the 3D gel culture. HCC–gelatin hydrogel cytocompatibility on SIOs enclosed in the structures was demonstrated by live/dead assay performed after 2 d and 8 d of culture (Figure XI).

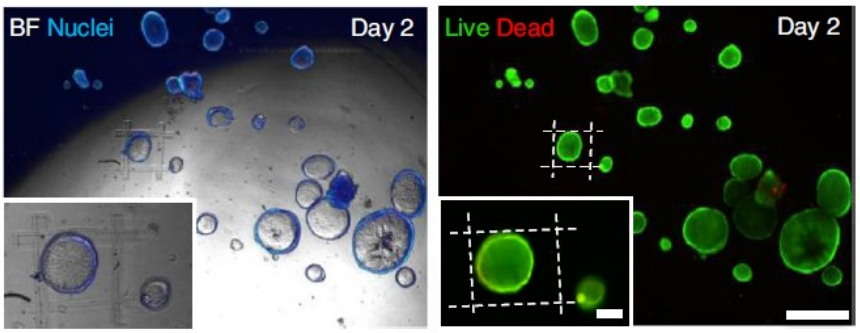

Figure XI. Creating structures in Matrigel/HCC gelatin mixture. Representative bright-field and fluorescence images showing live (green, calcein stained) and dead (red, ethidium homodimer-1 stained) cells in SIO cultures after 48 hours (400 μm scale). The insert shows a higher magnification of an organoid included in the structure crosslinked (scale 50 μm). The dotted lines indicate the position of the hydrogel.

Next, we investigated whether HCC–gelatin walls bioprinted in Matrigel and specifically positioned around individual SIOs could affect their behavior. SIOs confined in an open

square box (formed by four orthogonal walls) grew normally, and after few days of culture, touched and deformed HCC–gelatin hydrogel walls (Figure XII).

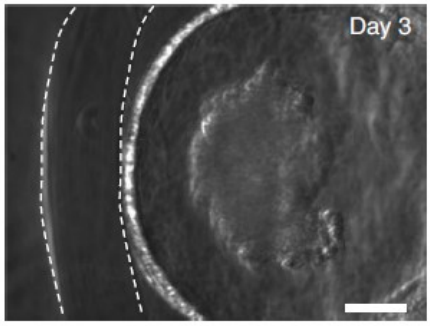

Figure XII. Representative images showing the morphology of a SIO enclosed by HCC–gelatin 3D-printed structures after 3 d in culture. Hydrogel was deformed by the organoid. Dashed lines indicate the position of hydrogel walls. Scale bar, 50 µm.

Between day 6 and day 8 of culture, SIOs enclosed in HCC–gelatin-based hydrogel showed marked changes in morphology, which led to well-developed columnar epithelium (Figure XIII a). This morphology was characterized by thickening of the organoid wall, F-actin localization in the apical position and nuclei constriction in the basal domain, as quantified by the basal–apical distance ratio and the basal–apical axis (Figure XIII b-c). By contrast, SIOs cultured in the same hydrogel composition but not in contact with HCC–gelatin structures did not show such morphological changes.

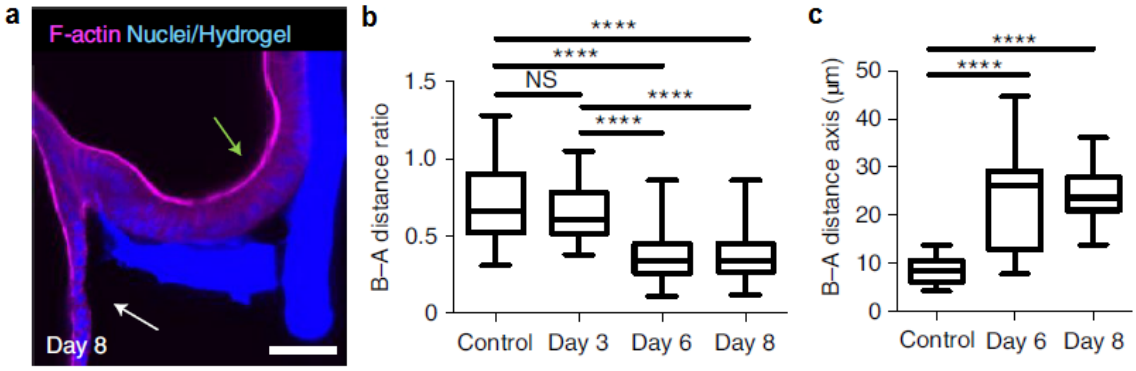

*Figure XIII. **a**. Confocal fluorescence image showing F-actin (magenta) organization in SIOs after 8 d of cell culture. The green arrow indicates a SIO enclosed in HCC–gelatin hydrogel (blue). The white arrow indicates a nearby organoid not enclosed by the hydrogel. Nuclei were stained with Hoechst (blue). Scale bar, 50 µm. **b**, Quantification of nuclear basal–apical (B–A) distance ratio and **c**, Quantification of the major basal–apical axis length of SIOs in standard*

*culture conditions (control) or enclosed by Matrigel–HCC–gelatin hydrogels at day 6 and 8 of cell culture. Data are shown as mean ± s.d. of 3 independent replicates; one-way ANOVA with Tukey's multiple-comparisons test; ****P < 0.0001.*

Interestingly, the basal localization of β4 integrin observed in SIOs enclosed in HCC–gelatin structures (Figure. XIV) suggests that cell adhesion could be a possible mechanism involved in the observed phenotype.

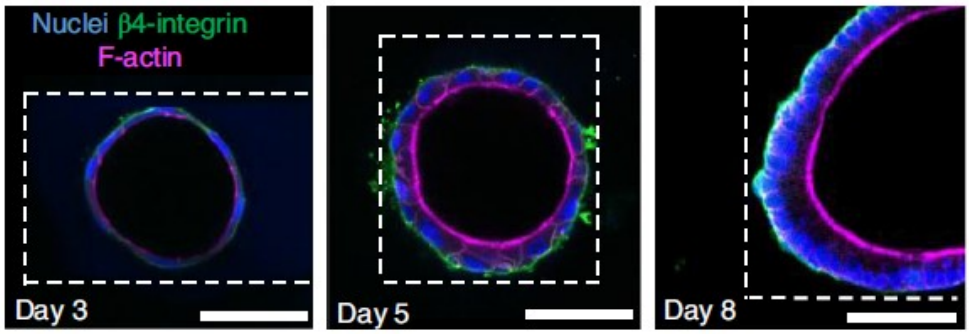

Figure XIV. Immunofluorescence of β4 integrin (green) and F-actin (magenta) in SIOs enclosed in Matrigel–HCC–gelatin hydrogels at day 2, 5 and 8 of cell culture. Dashed lines indicate the hydrogel position. Scale bar, 25 μm.

To dissect the contributions of extrinsic mechanical versus biochemical signals in triggering the organoid morphological changes, SIOs cultured in Matrigel were enclosed in an open square box made of HCC-8-arm PEG-based hydrogel, which is known to have cell-repellent properties [62, 63]. We show that HCC–8-arm PEG–Matrigel allowed SIO survival and growth in culture (Figure XV).

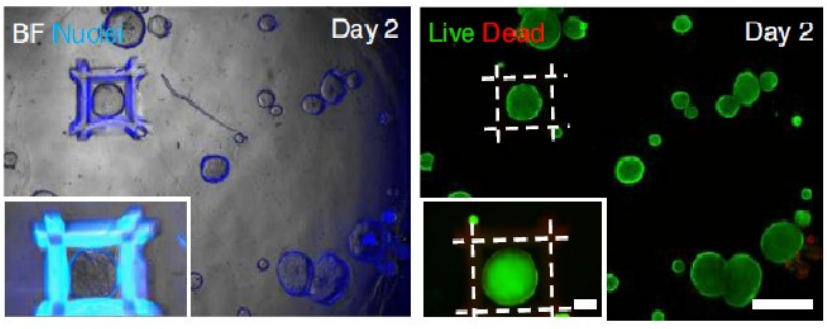

Figure XV. Representative bright-field and fluorescence images showing live (green, calcein stained) and dead (red, ethidium homodimer-1 stained) cells in SIO cultures 2 d after Matrigel–

HCC–8-arm PEG hydrogel photo-crosslinking. Scale bar, 400 μm. Inset shows a higher magnification of the organoid enclosed in the Matrigel–HCC–PEG hydrogel structure. Scale bar, 50 μm. Δz = 300 μm. Dashed lines indicate the position of the hydrogel.

However, unlike the observations with HCC–gelatin, SIOs enclosed in HCC–8-arm PEG-based hydrogel did not exhibit columnar epithelium after 8 d of culture, hydrogel deformation, actin apical localization or nuclei constriction (Figure XVI). Instead, the morphology of the SIOs reflects the 3D shape of the enclosed open box made by HCC–8-arm PEG-based hydrogel.

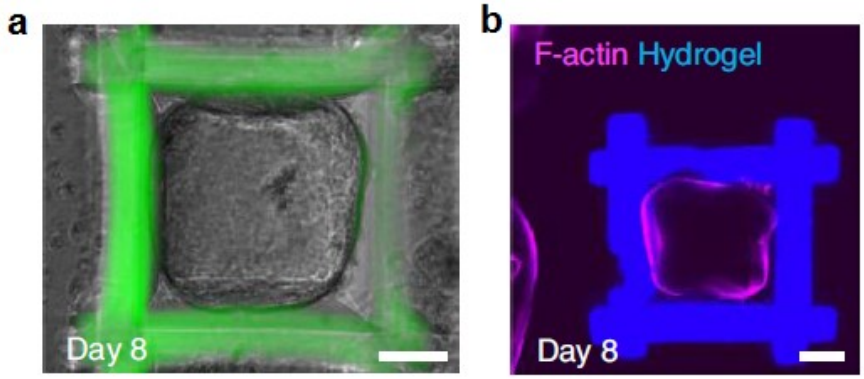

Figure XVI. ***a.*** *Representative images showing the morphology of a SIO enclosed in HCC–PEG 3D-printed structures after 8 days in culture.* ***b****, Fluorescence imaging showing actin (magenta) localization and hydrogel localization of a SIO enclosed by HCC–8-arm PEG 3D-printed structures after 8 days in culture. Nuclei were stained with Hoechst (blue). Scale bar, 50 μm*

Mechanical properties of synthetic hydrogels have a role in expansion and differentiation of mouse SIOs [64], whereas the effect of hydrogel stiffness on human SIO behavior remains unclear. Our results suggest that the formation of SIO columnar epithelium could be correlated to the biochemical composition of the hydrogel rather than its purely mechanical properties, since the HCC–gelatin and HCC–PEG share the same Young's modulus. It will be of interest to use this approach in future studies to investigate the cues that give rise to columnar epithelium in SIOs.

Creation of a GMP-compliant hydrogel

We then aimed to create a cell culture condition that was compliant with GMP regulation in order to eventually be able to translate the use of organoids *in vivo*. To optimize a GMP-compatible process for ECM gel, a 5-steps protocol was designed (Figure XVII), consisting of:

1) tissue harvesting;
2) decellularization;
3) freeze dry and milling;
4) gamma-irradiation and digestion;
5) neutralization

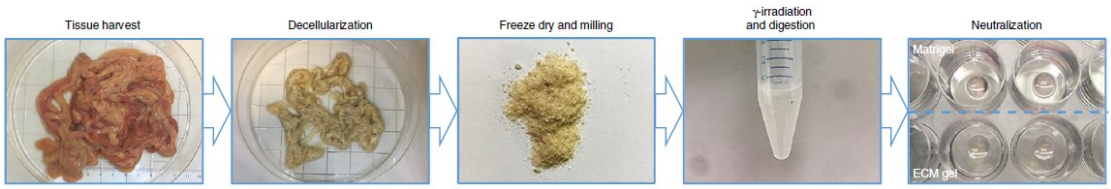

Figure XVII: The gelation preparation protocol consists of decellularization of the SI mucosa/submucosa, freeze-drying process, milling into a fine powder, gamma-irradiating and digesting the powder in pepsin and HCl for 72 h, and neutralization to a physiological pH, salinity and temperature.

Some of those steps rely on modification of previously reported protocols [57]. One cycle of the detergent-enzymatic treatment (DET) facilitated nuclei removal and significant DNA decrease in the porcine intestinal scaffold, with a median DNA content dropped from 143 ng/mg (SD 110) to 10 ng/mg (SD 5), below the limit considered to be indicative of complete removal. This short protocol minimized morphological tissue alteration compared to other decellularization protocols, as confirmed by the stainings performed for ECM (Fig. XVIII). Eventually, the removal of antigenic cellular material appears to be complete with a high preservation quality of extracellular matrix proteins after the process of decellularization, similarly to what has been previously reported [57].

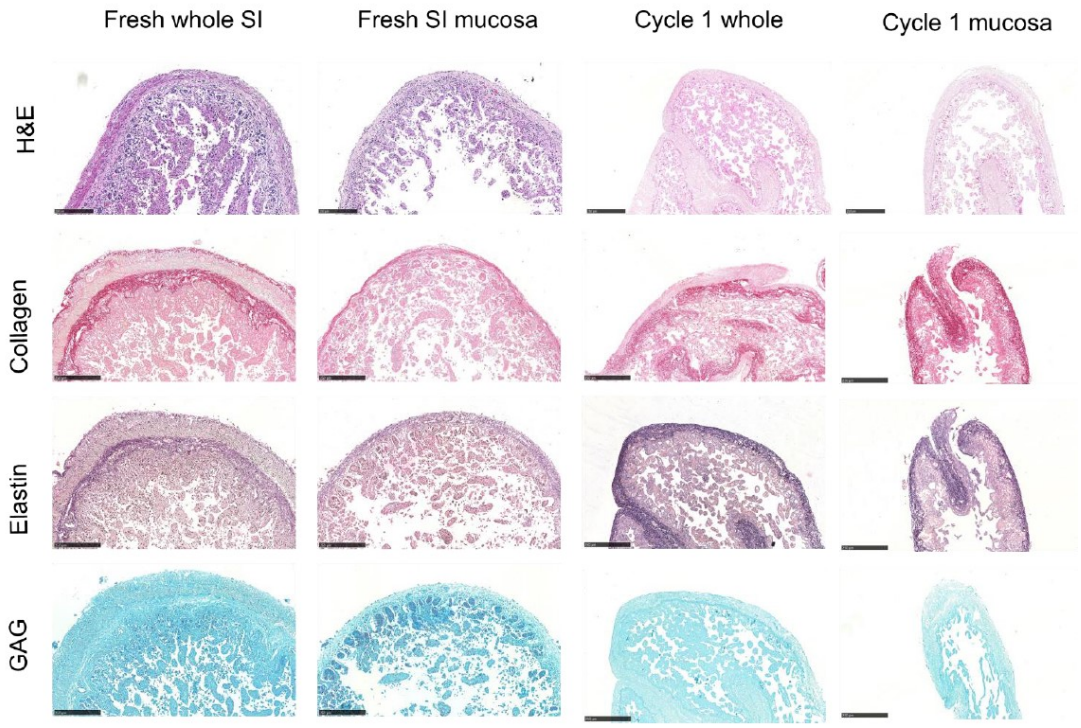

Figure XVIII. Sus scrofa small intestine sections pre- and post-decellularization staining. Hematoxylin/eosin, Picrosirius Red, Verhoeff's and Alcian Blue for cell nuclei, collagen, elastin and glycosaminoglycans, respectively. Scale bars 250 µm.

The ECM powder derived from porcine intestinal tissue successfully formed a hydrogel following a gelation protocol. ECM powder was digested in pepsin and HCl, re-equilibrated to neutral pH and exposed to physiological temperature. The SI ECM decellularization and gelation efficiently preserved the relevant ECM components including collagens, elastin and still contained glycosaminoglycans, which may be useful to instruct cells (Fig. XIX). Collagen content in ECM gel shows a paradox significant increase of 27.81 µg/mg ± 4.65 compared to fresh tissue 13.92 µg/mg ± 3.64 (mean ± SD); this increase compared to tissue weight, consistent with what has already been reported in the literature, is due to the loss in cytoplasmic compartment and different composition of the decellularized tissue which is constituted only by proteins of the matrix once decellularized. Elastin (ECM gel 4.14 µg/mg ± 1.65 vs fresh tissue 3.03 µg/mg ± 0.51) and glycosaminoglycans (ECM gel 0.51 µg/mg ± 0.26 vs fresh tissue 0.91 µg/mg ± 0.48) are anyhow maintained.

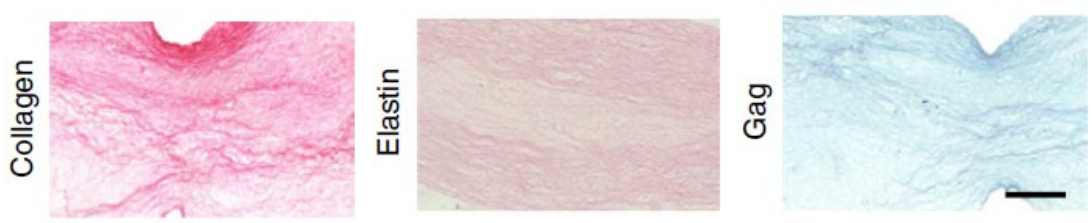

Figure XIX. Histological sections of fixed ECM gel drops stained with Picrosirius Red, Verhoeff's and Alcian Blue for collagen, elastin and glycosaminoglycans, respectively. Scale bar 200 μm

When compared to standard 3D culture systems, such as Matrigel, collagen I, III, and IV, the main collagen subclasses, showed at least comparable signals (Fig. XX).

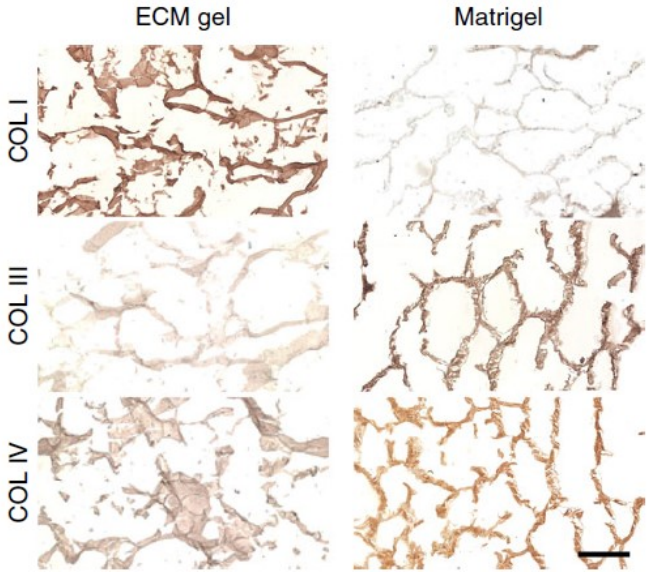

Figure XX. Analysis of the collagen types in ECM gel and Matrigel by staining for collagen I, III, and IV. Scale bar 100 μm.

Solubilization of ECM by pepsin digestion was performed to preserve the ultrastructure of the collagen fibers, based on the fact that pepsin cleaves collagens in locations where the three alpha-chains are not interacting to form a stable triple-helical structure [65]. To further investigate the structure of the ECM hydrogels, scanning electron microscopy (ESM) was performed and showed the detailed interwoven network of collagen fibers (Fig. XXI).

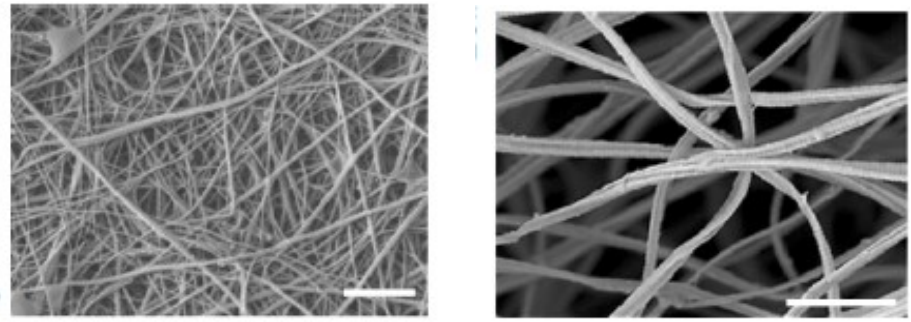

Fig. XXI. Scanning electron microscopy (SEM) images of the ECM gel displaying the interconnected fibrous network. Scale bars 1 µm.

Rheological and mechanical properties of 3D environment, which are extremely relevant to organoid culture, were also assessed by appropriate methods [66].

ECM gel allows an efficient human GI organoid culture

With the aim of obtaining a GMP-compliant cell culture, the ECM gel obtained was then used to isolate and grow GI organoids.

We initially used the ECM gel for the isolation and creation of organoids deriving from human biopsies, as shown in Figure XXII. Human organoids of gastric origin showed high level of adaptation to the SI ECM gel, with the possibility of obtaining organoids of comparable appearance to those isolated using Matrigel as a primary three-dimensional support.

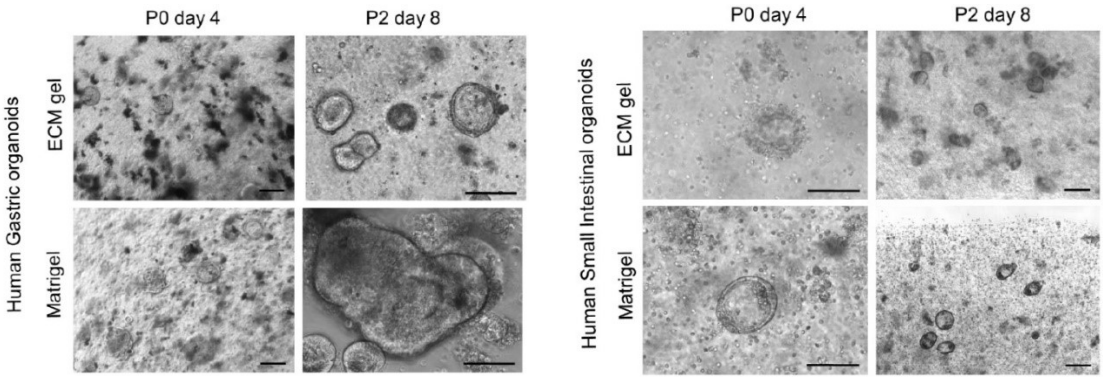

Figure XXII. Direct derivation of human gastric organoids, and human small intestinal organoids, from pediatric donor biopsies in 4 mg/mL small intestinal ECM gel and Matrigel control. Scale bars 200 µm

To confirm this data, human gastric organoids were grown entirely in ECM gel, showing a high level of adaptation to it, maintaining both the expression of epithelial markers (such as zonula occludens-1 ZO- 1, epithelial cadherin E-CAD and f-actin ACT) and properly gastric (such as ezrin EZR and mucin-5AC MUC5AC) after 7 days in culture (Figure XXIII).

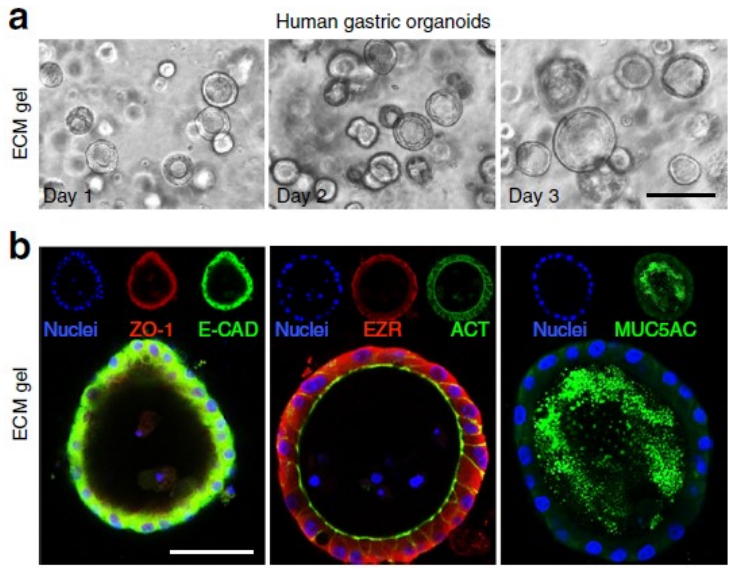

Figure XXIII. ***a****. Human pediatric gastric enteroids in ECM gel. Scale bar 200 µm.* ***b.*** *Planes of whole-mount immunofluorescence of 7-days gastric organoids showing both epithelial (zonula occludens-1, epithelial cadherin and actin) and gastric (ezrin and mucin-5AC) markers. Scale bar 50 µm.*

Similarly, the ability to form intestinal organoids and their characteristics are maintained when grown in ECM gel compared to Matrigel. In particular, human organoids grown in ECM gels showed a proportion of living cells similar to those grown in Matrigel, confirming a high cytocompatibility (Figure XXIV).

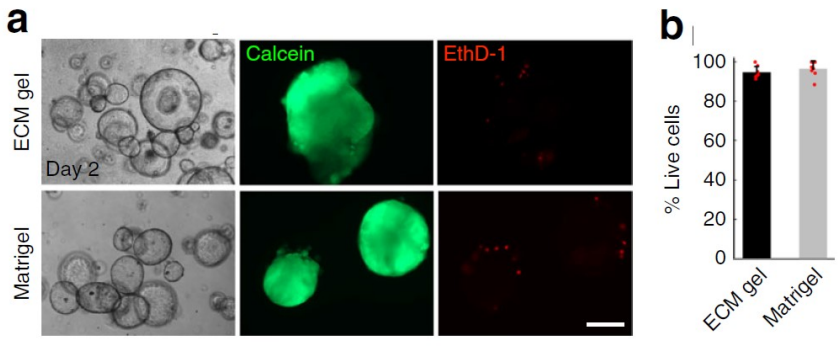

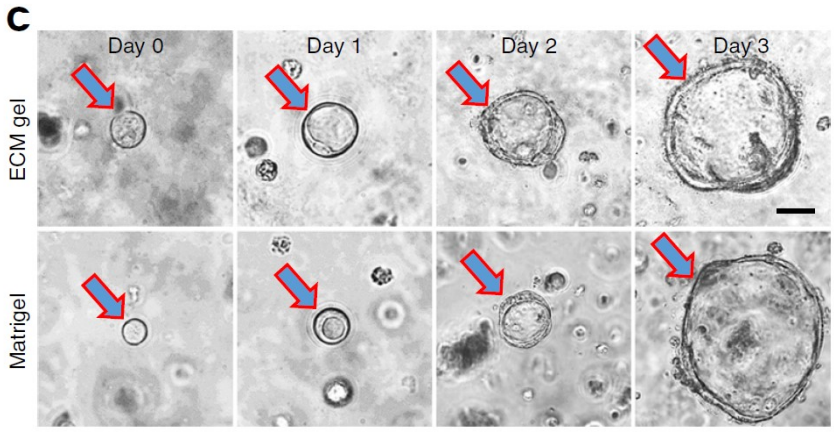

Figure XXIV. ***a****. Live/Dead assay of human pediatric SI organoids cultured in ECM gel and Matrigel. Calcein-AM shows living cells. Ethidium homodimer-1 shows dead cells. Scale bar 200 µm.* ***b*** *Quantification of vital cells from Live/Dead assay. Mean ± S.D. (n =8 organoid cultures).* ***c****. Single-cell colony (arrows) formation capacity assessed over 3 days in disaggregated human fetal SI organoids in ECM gel and Matrigel. Scale bar 25 µm.*

Organoids grown in ECM gels maintain good differentiation capacity in intestinal phenotype, as confirmed by the expression of crypt markers (olfactomedin-4 OLFM4 and lysozyme LYZ) and villi (cytokeratin 20 CK-20 and actin ACT), as shown in figure XXV.

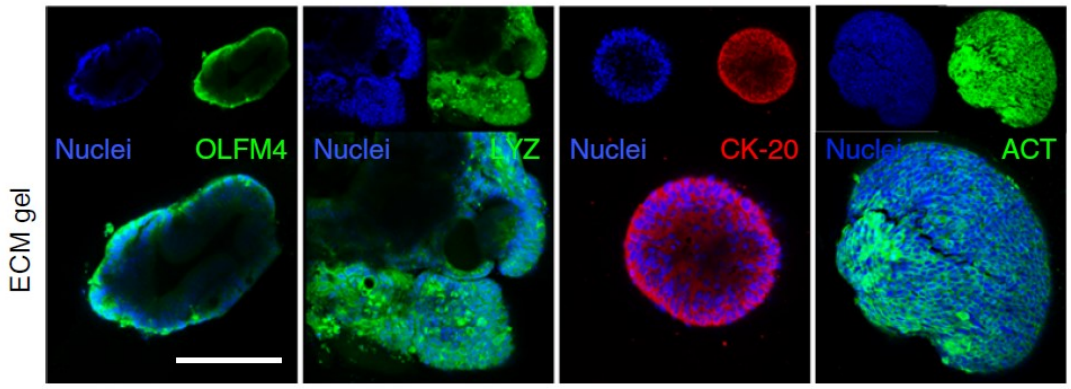

Figure XXV. Whole-mount immunofluorescence of human fetal SI organoids showing crypt stem cell marker olfactomedin-4 OLFM4, crypt Paneth cell marker lysozyme LYZ, villi enterocyte marker keratin-20 CK-20 and actin ACT staining. Scale bar 100 µm.

The cell culture was of excellent quality for the first passages, with organoid sizes comparable to those grown in Matrigel. However, if kept in culture for a medium-long

time, i.e. for about 2 months, in the last passages there was a slight decline in the morphological characteristics of the organoids (Figure XXVI). To obviate this may be useful to further investigate the possibility to load the gel with other stimulating factors.

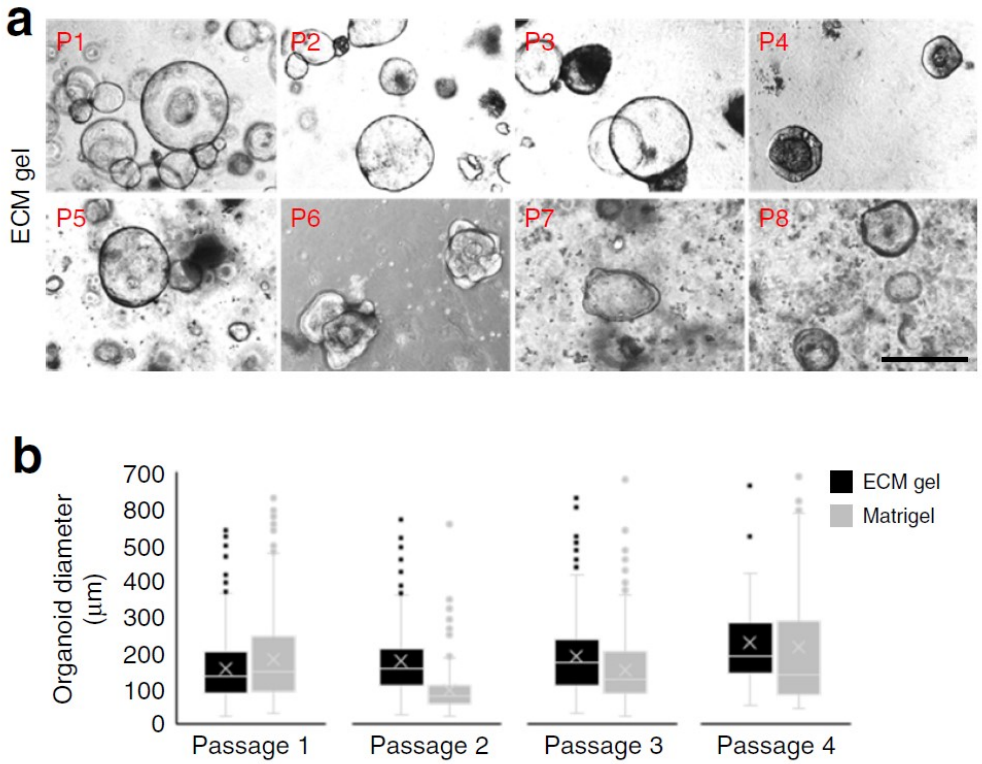

Figure XXVI. ***a****. Morphology of eight consecutive passages over a period of 2 months of human pediatric SI organoids in ECM gels. Scale bar 300 µm.* ***b****. Analyses of four consecutive passages of human pediatric SI organoids diameters at day 3 of culture in ECM gel and Matrigel. Mean ± S.D. (n ≈ 200 organoids).*

GI with reverse polarity facilitates expression of receptors on the external surface

In order to validate gastric organoids as functional *in vitro* models of SARS-CoV-2 infection and replication, we optimized the culture condition for viral infection in a 3D system. Standard organoids of endodermal organs have a luminal polarity facing the internal portion of the structure, with an apical (inner) f-actin and zonula occludens-1 (ZO-1), and basal external lamina marked by β-4 integrin (β4-INT) (Figure XXVII-VIII).

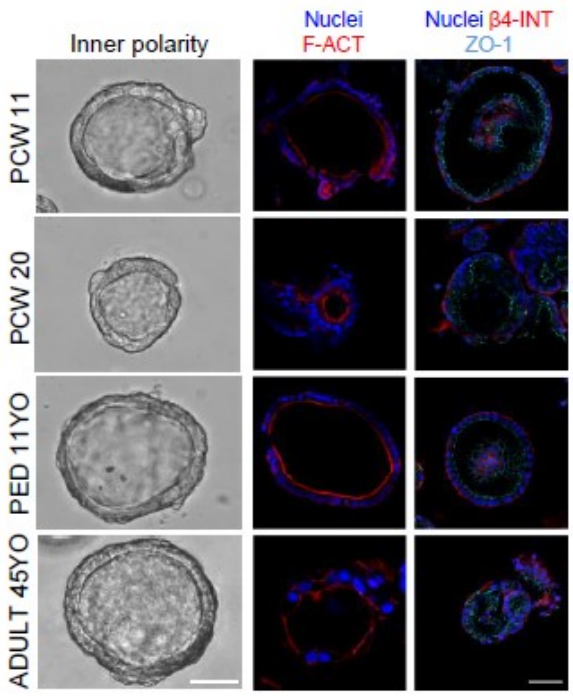

Figure XXVII. Gastric organoids with normal (inner) polarity and large lumen. Immunofluorescence panel showing f-actin (F-ACT) in red, zonula occludens-1 (ZO-1) in violet, β-4 integrin (β-4 INT) in red, and nuclei in blue (Hoechst). Scale bar 50 µm.

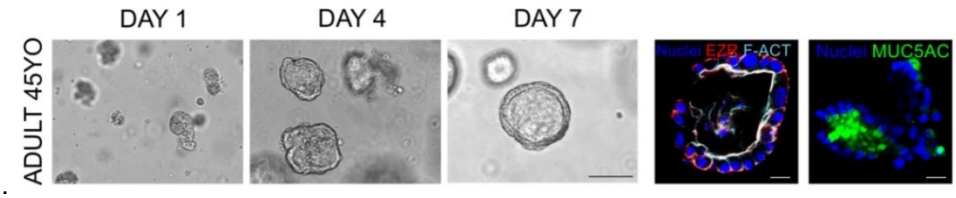

Figure XXVIII. Immunofluorescence panel for adult 45 years-old patient organoids showing ezrin (EZR) in red, f-actin (F-ACT) in cyan, mucin 5AC (MUC5AC) in green and nuclei in blue (Hoechst). Scale bars 25 µm.

To maximize the efficiency of infection, we reverted the polarity of gastric organoids (RP-GO) [56] to expose the apical side of the cells on the outer side. Organoids were removed from the surrounding extracellular matrix and cultured in suspension for 3 days, resulting in the exposure of the apical f-actin on the outer side, accompanied with MUC5AC secretion externally (Fig. XXIX). ZO-1 and β4-INT expression was also inverted compared to standard organoids in Fig XI.

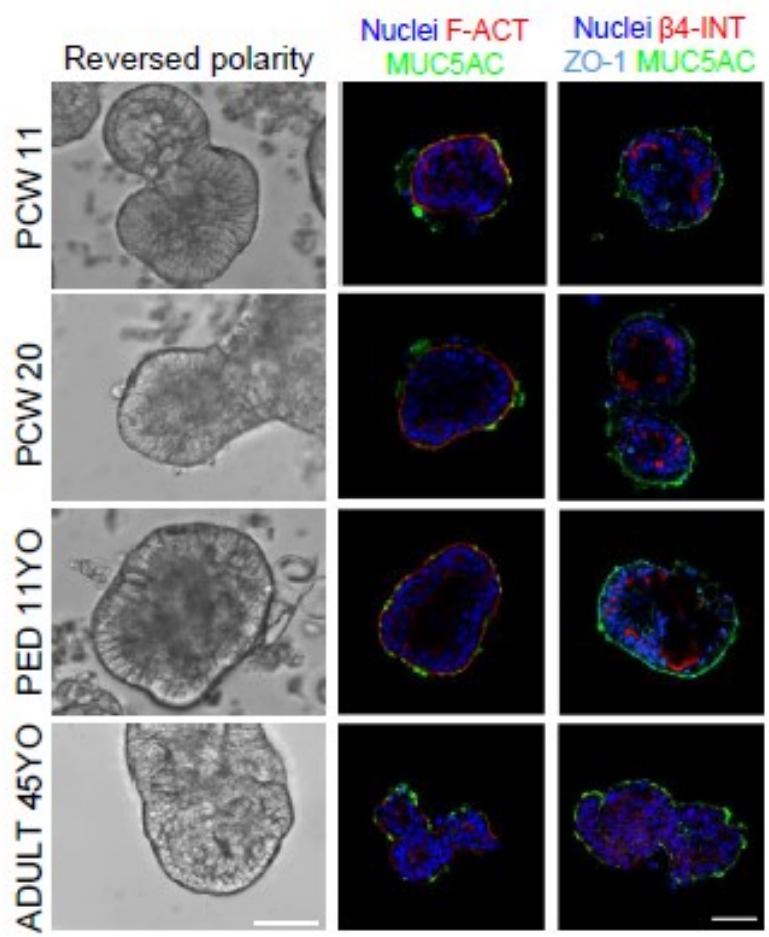

Figure XXIX. RP-GOs showing an almost absent lumen. Immunofluorescence panel showing f-actin (F-ACT) in red, zonula occludens-1 (ZO-1) in violet, β-4 integrin (β-4 INT) in red, mucin 5AC (MUC5AC) in green and nuclei in blue (Hoechst). Scale bar 50 µm.

Full 3D deconvolution images of reverse organoids are shown in Fig. XXX.

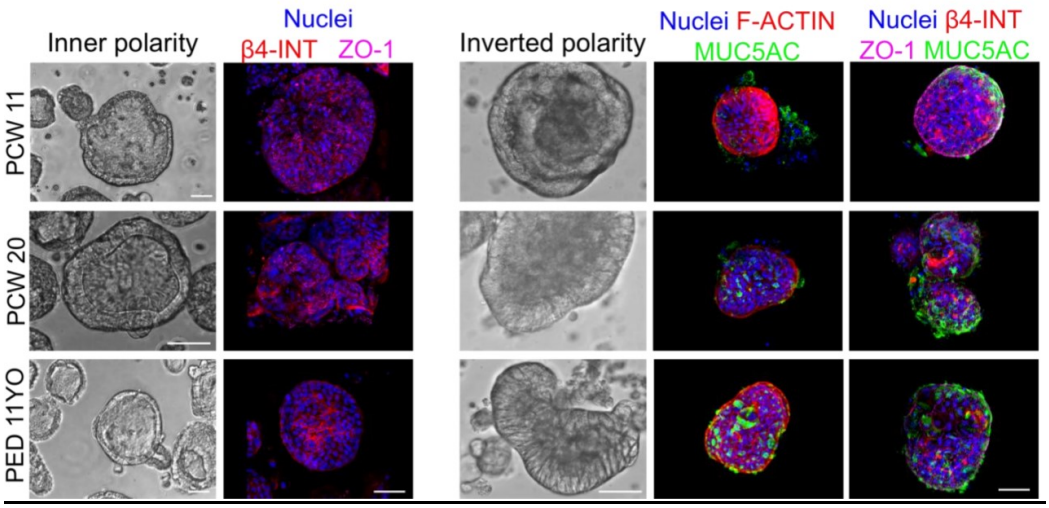

Figure XXX. 3D Deconvolution confocal images. (Left) Gastric organoids with normal inner polarity lumen. Immunofluorescence panel zonula occludens-1 (ZO-1) in violet, β-4 integrin (β-4 INT) in red, and nuclei in blue (Hoechst). Scale bars 50 µm. (Right) Gastric organoids with reversed polarity, showing an almost absent lumen. Immunofluorescence panel showing f-actin (F-ACT) in red, ZO-1 in violet, β-4 INT in red, mucin 5AC (MUC5AC) in green and nuclei in blue (Hoechst). Scale bars 50 µm.

Principal component analysis (PCA) on organoid RNA sequencing data showed similar clustering among the different stages of normal polarity organoids and RP-GOs (Figure XXXI).

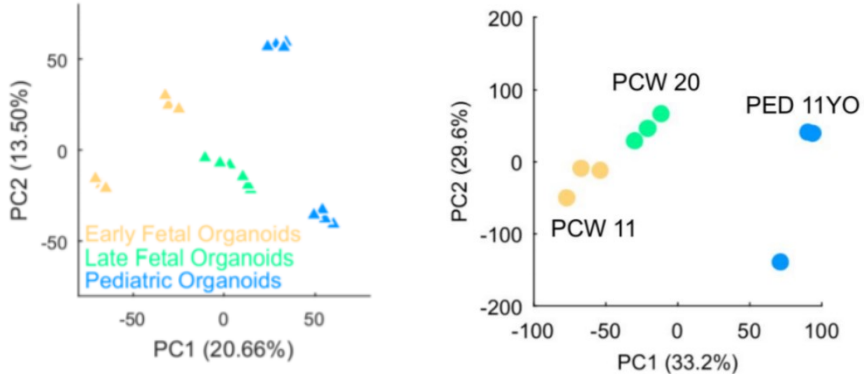

Figure XXXI. (Left) Principal Component Analysis (PCA) of RNA-seq organoid samples at different stages of development as indicated. Stages of tissue of origin for organoid derivation: early fetal (week 8-15), late fetal (week 17-20) and pediatric. (Right) same analysis from RP-GOs at different stages of development.

We then analyzed the absolute expression of *ACE2* and transmembrane protease serine 2 (TMPRSS2) in our newly developed gastric models of fetal and pediatric origin and in the tissues of origin, as those are known to be crucial in SARS-CoV2 infection. RNA-seq data analysis showed that expression of *ACE2* was significantly lower in early fetal stomachs compared to the pediatric ones, while late fetal samples' higher variability, not allowing us to draw a conclusion.

On the other hand, *TMPRSS2* mRNA expression was consistently high in all stomach samples irrespective of stages. In RP-GOs, the expression profiles for *TMPRSS2* were similar across all stages, while for *ACE2*, RP-GOs of adult and pediatric origin recorded the lowest and the highest levels, respectively. Organoids of fetal origin had similar intermediate counts that were significantly lower than the pediatric ones (Fig. XXXII).

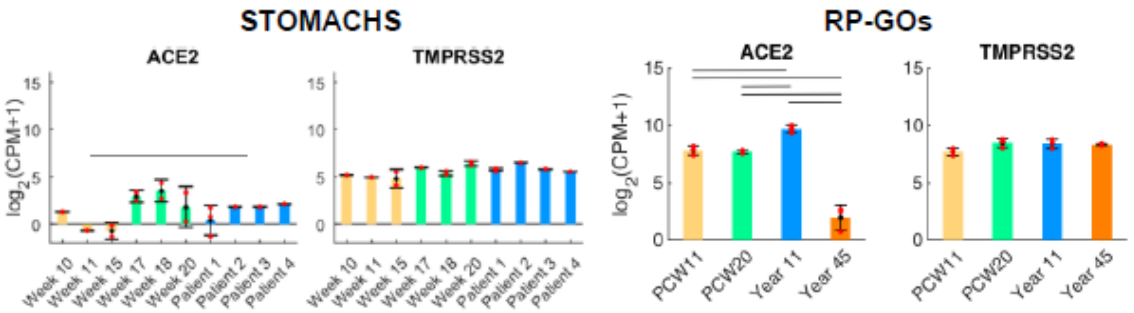

Figure XXXII. SARS-CoV-2 receptors, angiotensin-converting enzyme 2 (ACE2) and transmembrane protease serine 2 (TMPRSS2) absolute RNA-seq expression in gastric tissues (left) and gastric organoids (right). Mean ± SD (n≤3 for tissues biological replicates, n=3 for organoids). CPM: count per million.

While presence of ACE2 and TMPRSS2 proteins had already been shown for the adult stomach [67], we confirmed their expression by immunofluorescence staining in fetal and pediatric gastric biopsies (Fig. XXXIII).

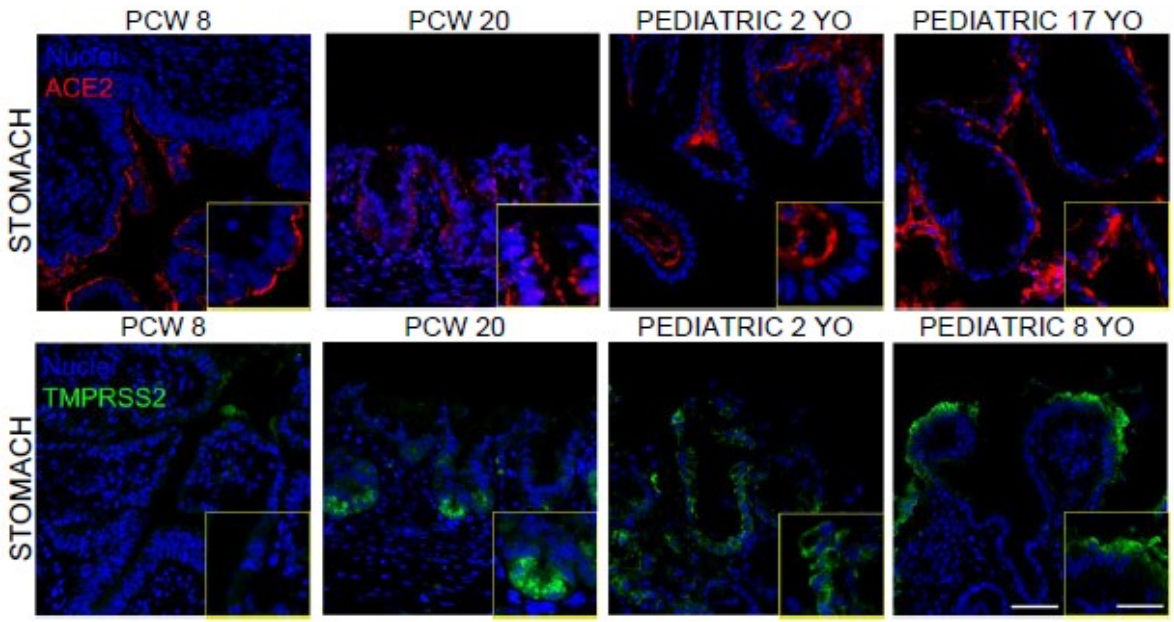

Figure XXXIII. Immunofluorescence panel showing ACE2 in red, TMPRSS2 in green and nuclei in blue (Hoechst) in fetal and pediatric stomach biopsies. Scale Bar 50 µm (main figures) and 30 µm (enlargement).

Similarly, their co-presence in all of the RP-GOs derived at PCW11, PCW 20, pediatric and adult stages was proven (Fig. XXXIV).

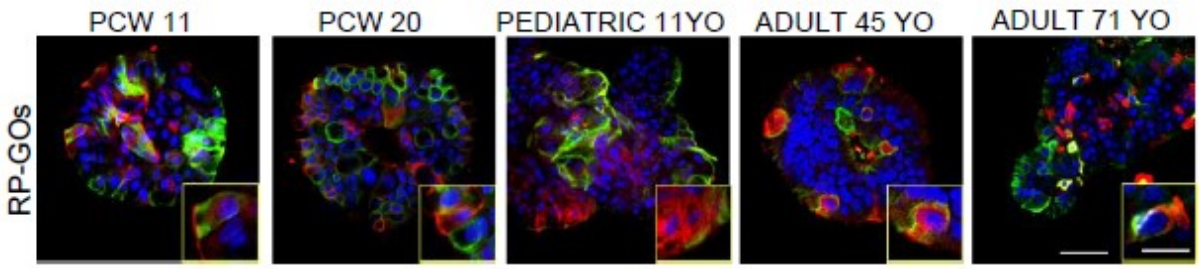

Figure XXXIV. Immunofluorescence panel showing ACE2 in red, TMPRSS2 in green and nuclei in blue (Hoechst) in fetal, pediatric, and adult gastric organoids with reverse polarity. Scale bar 30 µm (main figures) and 10 µm (enlargement).

GI organoids as a model of *in vitro* SARS-CoV2 infection

To evaluate the susceptibility of both normal and reverse polarity organoids to SARS-CoV-2 we first conducted a study with fetal and pediatric organoids. Normal polarity fetal and pediatric gastric organoids embedded in Matrigel were readily infected by SARS-CoV-2, as demonstrated by the presence of viral double-stranded RNA (dsRNA) in the cytosolic compartment of cells (data not shown). A parallel comparison across fetal, pediatric, and adult age organoids was conducted using
RP-GOs. After a 2-hour infection, organoids were cultured up to 96 hours in suspension and checked for structural integrity and viability by visual examination on a daily basis (Fig. XXXV).

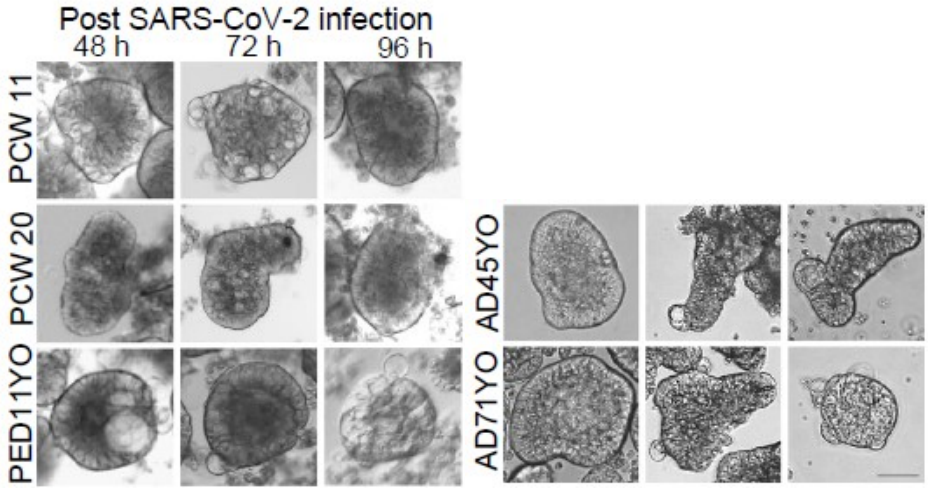

Figure XXXV. Bright field images of RP-GOs infected with pediatric patient-derived SARS-CoV-2 for 2 hours, and acquired at 48, 72 and 96 h post-infection. Scale bar 50 µm.

Immunofluorescence staining of the coronavirus nucleoprotein (NP CoV) and dsRNA (Figure XXXVI-XXXVII) indicated the susceptibility to infection of all organoids irrespective of the donors' age.

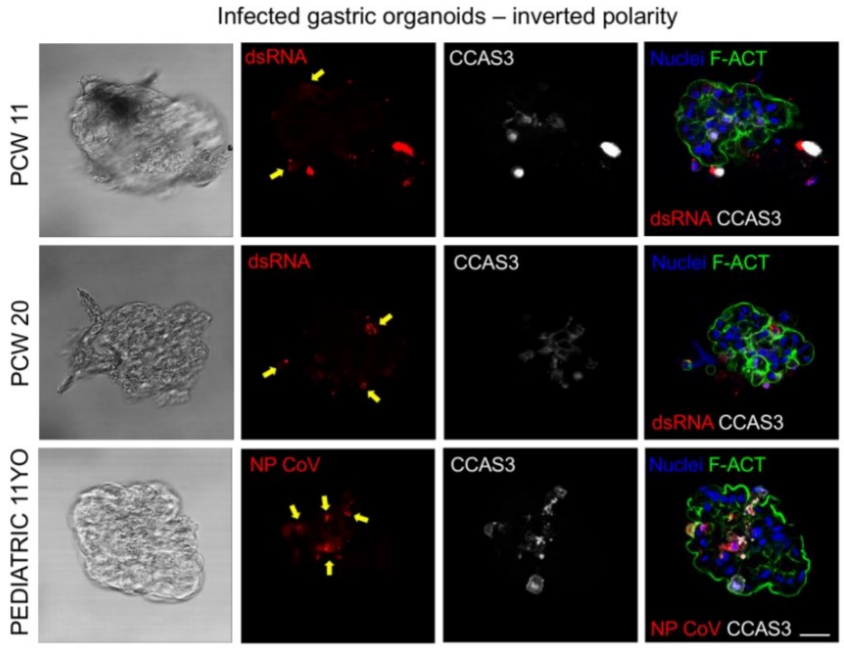

Figure XXXVI. SARS-CoV-2 staining at 96 h post-infection in reversed-polarity gastric organoids. Immunofluorescence panel showing viral double strand RNA J2 (dsRNA) in red, SARS-CoV-2 Nucleocapsid Antibody (NP CoV) in red, cleaved caspase 3 (CCAS3) in white, f-actin (F-ACT) in green and nuclei in blue (Hoechst). Scale bar 50 µm.

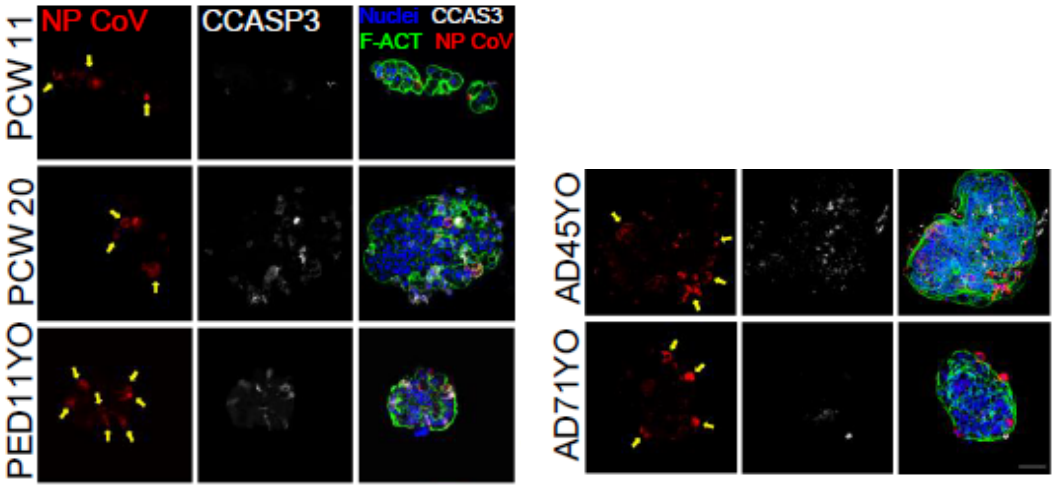

Figure XXXVII. Infected cells in RP-GOs fixed at 96 h post-infection. Immunofluorescence panel showing SARS-CoV-2 Nucleocapsid Antibody (NP CoV) in red, marking infected cells (yellow arrows), cleaved caspase 3 (CCAS3) in white, marking apoptotic cells, f-actin (F-ACT) in green and nuclei in blue (Hoechst). Image is representative of at least 5 similar organoid images. Scale bar 50 µm.

Interestingly, NP CoV was detected in the same cells where cleaved caspase 3 (CCAS3) was observed, indicating that SARS-CoV-2 infected gastric cells undergo programmed cell death (apoptosis), as shown in Figure XXXVIII.

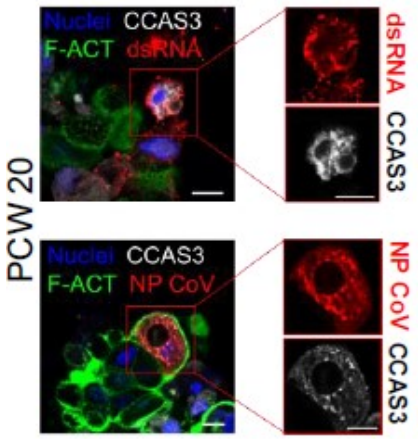

Figure XXXVIII. Infected cell details in RP-GOs fixed at 96 h post infection. Immunofluorescence panel showing viral double strand RNA J2 (dsRNA) in red, SARS-CoV-2 Nucleocapsid Antibody (NP CoV) in red, cleaved caspase 3 (CCAS3) in white, f-actin (F-ACT) in green and nuclei in blue (Hoechst). Scale bars 10 µm.

We then analyzed the yield of infectious progeny virus and genome copies in culture supernatants collected at 0, 24, 48 and 72 hours post-infection. Pediatric and late fetal RP-GOs recorded the highest infectious titers, with peak values of 104 FFU/ml, at 72 hours post-infection, significantly higher than early fetal and adult stage organoids, for whom the majority of values was either below or around the limit of detection of the FFA. (Figure XXXIX).

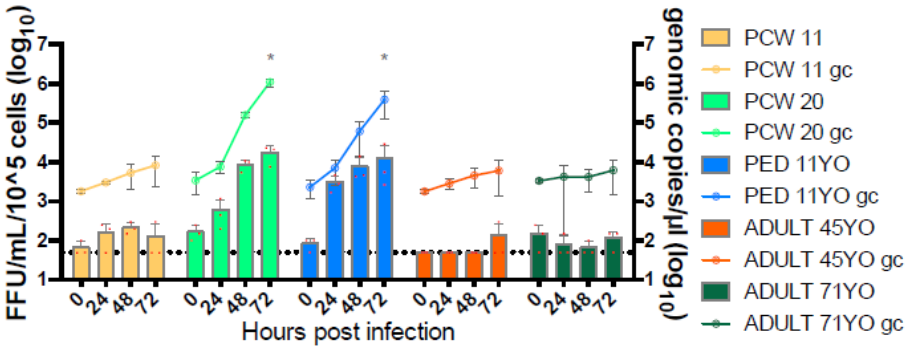

Figure XXXIX. Graph of SARS-CoV-2 replication in fetal, pediatric and adult undifferentiated RP-GOs. Live virus yield was titrated by FFA on Vero E6 cells of culture supernatants collected

at 0, 24, 48 and 72 hours after infection with SARS-CoV-2 (MOI of 0.5). The dotted line indicates the lower limit of detection. Red dots indicate single data points. Mean ± SD (N=3).

To confirm the poor susceptibility of adult undifferentiated organoids, we repeated the experiment with the 45 years-old RP-GOs, using both the standard (MOI of 0.5) and a 10X challenge dose (MOI of 5). In this experiment, we observed temporary modest increases in genome copies, but we could not detect infectious viral progeny in the supernatant (Figure XL).

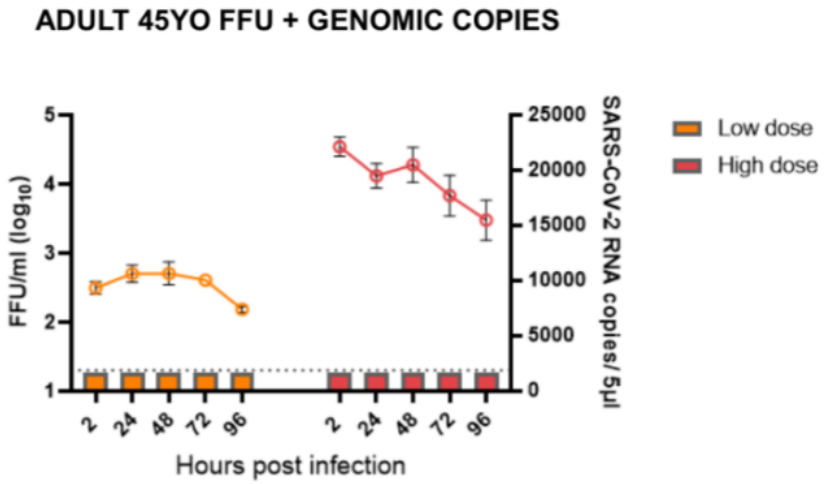

Figure XL. Graph of SARS-CoV-2 replication in adult RP-GOs, showing Focus Forming Units (FFU) and genomic viral RNA copies, in low (MOI of 0.5) and high (MOI of 5) dose of infection. The dotted line indicates the lower limit of detection. Mean ± SD (N=3).

DISCUSSION

From Gastrointestinal Epithelium development to Organoids formation

Gastrointestinal epithelium development and differentiation is controlled by a complex interplay of signaling pathways and transcriptional factors, defying the so called epithelial-mesenchymal crosstalk. After birth, the continuous cell turnover requires the persistent activity of stem cells, which also rely on this interaction to be maintained. An understanding of the timing of epithelium formation in the fetal life might be useful in the organoid research as their *in vitro* differentiation may recapitulate the same steps and, moreover, the mechanisms behind the development of an organ may be translated into the dish to efficiently promote and maintain the culture.

Despite the steps of formation and differentiation of the intestinal epithelium are well known, the stomach has been so far less studied. Evolutionarily, the stomach as a functional organ, with its acid and digestive enzyme-secreting properties, emerged well after the development of the intestine. Its final maturation into the adult form slowly occurs; for example, in rodents it is achieved several weeks after birth. Therefore, we firstly studied gastric epithelium differentiation and specification throughout fetal life, defying precise gestational ages for each cell type to reach full maturation.

Furthermore, as a reliable 3D culture *in vitro* model of human gastric mucosa at different developmental stages has been so far challenging to achieve, we then successfully derived human stomach organoids across developmental stages and studied their morphology and cell type differentiation and maturation. Those results were compared to the tissue morphology leading to a precise patterning toward gestational ages. The availability of a wide range of GI organoids, corresponding to all ages from fetal development to childhood, is a unique aid to answer any queries rising from clinical need in pediatrics and makes a potential translation to personalized medicine closer.

Gastrointestinal organoids and the Extracellular Matrix

The ECM is a complex 3D microenvironment that surrounds cells and it both provides support for tissue integrity and elasticity and transmits biochemical signals that regulate cell differentiation, proliferation and survival. Its composition varies between organs, but it is mainly constituted of water, proteins (collagen, elastin, fibronectin, and laminin), and polysaccharides [68]. Cells actively interacts with the surrounding ECM with the first secreting and remodeling the ECM and the latter inducing cell identity. This concept has been particularly used in defining the characteristics of the "niche", the microenvironment surrounding stem cells in which the ECM, along with soluble factors secreted by mesenchymal cells, provides specific biophysical and biochemical stimuli that maintain stemness [69].

The presence of a 3-dimensional structure surrounding the cells growing in culture have to be kept in mind especially in the organoids field, as both the maintenance of the stemness and the completion of differentiation are culture end points. As for as the interaction between the growing organoid and the matrix *in vitro*, both biological and mechanical factors have to be considered. Stem cell differentiation is directly affected by the stiffness and elasticity of the ECM [70], as cell adhesion to the ECM through integrins or other proteins, results in signaling cascades that regulate gene expression and thus drive differentiation a proliferation [68].

Using a bottom-up approach to deconstruct the complexity of the ECM-organoid interaction, firstly we found that incorporation of crosslinked poly(ethylene glycol) (PEG)-external obstacles within the ECM enclosed to the organoid failed to support cell maturation within the organoid. Organoids modify their external shape to follow the constriction due to the presence of the obstacle but do not exhibit maturation signs. We postulated that this might be related to the cell-repellent properties of the PEG mixture.

As a further step we thus analyzed the interaction of the organoids with a less inert obstacle under the same condition. We decided to use for this second batch of experiments a mixture containing HCC (7-hydroxycoumarin-3-carboxylated). This led in few days in culture to the observation of an interaction between the organoid and the obstacle, with the former adhering to the HCC construct and progressively modifying both its global shape and cell characteristics. Indeed, adherent cell showed marked changes in

morphology toward a columnar epithelium, with thickening, F-actin localization in the apical position and nuclei constriction in the basal domain.
This proof of concept with the use of 3D bioprinting technology highlights the important influence of the ECM on organoid growing. Having the possibility to temporary modify the surrounding environment in pre-existing 3D cultures, may help understanding *in vitro* organoid models, instructing cell structural organization and driving differentiation.

Gastrointestinal organoids and the Extracellular Matrix: creating a bridge towards clinical applications

While research in the organoid field is leading to exciting findings with broad therapeutic potential, their clinical translation is still currently limited by the lack of GMP-compatible conditions for organoid derivation and expansion. The main obstacle is the need of a 3D structure that efficiently mechanically support cells growth and organoid expansion while providing necessary stimuli directing cell adhesion, survival, proliferation and differentiation. An ex vivo 3D cell culture support should ideally recapitulate aspects of this native microenvironment and facilitate these functions [71]. LGR5+ cells, isolated from the crypts of the intestine are an example of a cell type that favors a 3D environment for *ex vivo* culture over 2D [72], forming organoids if cultured under optimal conditions. We showed the development of an ECM naturally derived gel that have the potential to both direct and influence human organoids behavior *in vitro* and *in vivo* [66].
In literature, both natural and synthetic hydrogels have been examined for their ability to support organoid culture, each having its own associated advantages and limitations. Recently, synthetic alternatives to Matrigel have been reported [73]. While synthetic gels have the advantage of being GMP-compliant and fully reproducible, they are limited by a lack of biological signals provided to the cells. ECM is far more complex and it is not only a mere scaffold, but it is a determinant of tissue specificity itself.
The tissue development is not a cell autonomous process, but it is instead instructed by the surrounding environment [74]. As elsewhere mentioned, epithelial and mesenchymal components interact during development to direct tissue morphogenesis and differentiation. We demonstrated that DET protocol on porcine intestine tissue efficiently

remove all native tissue cells, as confirmed by both stainings and DNA quantification, while preserving crucial ECM components, such as collagen, elastin and GAGs. We identified that gelation was fastest in the 6 mg/mL concentration, which also had the rheology profile most similar to Matrigel [66].

The created ECM-gel allowed the isolation and growth of GI organoids similar to Matrigel. Notably, as a further step towards clinical translation of this protocol, we demonstrated the possibility to derive organoids directly from human biopsies without the use of Matrigel at the first passage after tissue dissociation. Furthermore, all the specific intestinal markers, defining both crypt and villi signature, were expressed in ECM gel compared to Matrigel cultured organoids, underlying the suitability of the ECM to host human cultures.

A translational application of ECM-derived hydrogels is currently hampered by the high variability of the lab-derived products. In our study, batch to batch variation was observed because of the biological origin of the gel. To better standardize the process, we always used animals with similar characteristics and created mixed batch of ECM powder. However, to further overcome this real issue, further studies are needed especially looking at the potential of combining the ECM hydrogel with synthetic molecules. For instance, Gjorevski et al [75] showed that enrichment of their synthetic PEG gel with major ECM components such as fibronectin enhanced mouse intestinal stem cell survival and proliferation. The same approach is likely to benefit this ECM gel in future development studies, particularly the addition of laminin, a key component of the basement membrane in the intestine [76]. In view of GMP-grade production for clinical use, it is important to underline that all the chemicals and reagents utilized during each step of the gel production pipeline are already commercially available at GMP-grade.

Long-term expansion requires stable and consistent cultures. During the experiments we observed a slightly reduced organoid growth after several passages, likely due to the accumulation of stiff ECM leftovers from previous passages. However, we observed comparable outcome during the first 3–4 passages, which would be sufficient for ex vivo cell expansion needed eventually for cell therapy.

Gastrointestinal organoids and the SARS-CoV2 infection: the prompt application of a novel culture model to an emerging clinical burden

To prove the clinical relevance of GI organoids in case of emergency clinical needs, we then experimented the response of the culture to SARS-CoV2 infection. As mentioned above, COVID-19 pandemic had a huge impact on the socioeconomic and clinical life over the last months. The use of fetal and pediatric derived organoids aimed to answer to two clinical scenarios: the investigation of the possible active infection through the gastrointestinal tract either in children (with fecal-oral transmission) or through vertical transmission in pregnant women.

With the aim to optimize the culture conditions to produce more reproducible data, we decided to avoid injection of the virus within the organoids and preferred to infect human gastric organoids under steady-state conditions. Direct injection mechanism is graved by a high inter-operator and inter-laboratory variability and thus both reduce repeatability and accuracy of the data. We thus decided to take advantage from the already available literature on organoid polarity reversion [56] and we generated cultures of RP-GOs in suspension of fetal, pediatric, and adult origin. We described how a reverse polarity organoid model can help exposing the apical domains, in direct contact with the surrounding microenvironment, so that pathogens can easily access surface receptors on the cells.

A crucial preamble to the infection of gastric organoids is that previous studies showed that angiotensin-converting enzyme 2 (ACE2) receptor is highly expressed on differentiated enterocytes and that intestinal organoids derived from the small intestine can be easily infected by SARS-CoV-2 [77]. ACE2 has been identified to be the main host cell receptor enabling SARS-CoV-2 cell entry after interaction with its surface glycoprotein S. Interestingly, intestinal organoids derived from both human and horseshoe bats are fully susceptible to SARS-CoV-2 infection and sustain robust viral replication.

In the condition of exposed apical polarity and absence of surrounding ECM support, as for the RP-GO culture, we demonstrated that the RP-GOs are fully susceptible to SARS-CoV-2 infection. Analyzing the infectivity of the progeny virus, we recorded infection level comparable to those shown by Zhou et al [78].

We furthermore observed that late fetal and pediatric organoids allow higher replication of the virus, while early fetal and adult organoids, although infected, released significantly lower amounts of infectious viral progeny, when cultured in expansion medium. Quantification of gene transcripts coding for the viral receptors ACE2 and TMPRSS2 suggested that the observed levels of replication could depend on differences in the density of ACE2 receptors. Although we could not run the same analysis on adult stomach biopsies, our data on ACE2 expression and susceptibility to infection are in keeping with the literature indicating that adult gastric cells express lower levels of ACE2 compared to intestinal cells [78].

Apoptosis is one of the key mechanisms of cells to restrict viral infections by destruction of the cellular machinery indispensable for virus replication. In RP-GOs, immunofluorescence staining for the nucleocapsid indicated a clear cytosolic localization of this protein that in some cells was associated with the presence of the cleaved caspase 3, confirming the occurrence of apoptosis in the gastric compartment [79]. This mechanism demonstrated in GI organoids might be easily translated to the whole infected GI epithelium (*in vivo* mucosa) and it might account at least in part for the frequent abdominal symptoms typical of the involvement in the COVID-19 pediatric patients, such as pain, vomit and diarrhea [80].

CONCLUSIONS

In conclusion, gastrointestinal organoid system offers a unique opportunity to *in vitro* model diseases. The optimization of well-established protocols from different developmental ages helped to develop a quick tool to answer clinical needs, as to characterize the replication of virus and postulate some of the pathological consequences of infection. This innovative model could represent an interesting platform for the development and testing of antiviral drug candidates targeting the GI system.

The clinical importance of our findings related to the SARS-CoV-2 infection is the worrisome phenomenon of prolonged shedding from the GI tract and suggests a possible risk of vertical transmission in infected pregnant women. Moreover, defining ages of susceptibility and identifying target anatomical sites will prove of crucial importance for the implementation of diagnostic screening for the identification of contagious asymptomatic patients.

PhD student
Dr. Elisa Zambaiti

REFERENCES

[1] Thoo L, Noti M, Krebs P. Keep calm: The intestinal barrier at the interface of peace and war. Cell Death Dis. 2019, 10, 849.

[2] Hsu Y-C, Fuchs E. A family business: Stem cell progeny join the niche to regulate homeostasis. Nat. Rev. Mol. Cell Biol. 2012, 13,103–114.

[3] Taeko KN, Donahue B, Shroyer NF. Intestinal development and differentiation. Exp. Cell Res. 2011, 317, 2702–2710.

[4] Zorn AM, Wells JM. Vertebrate Endoderm Development and Organ Formation. Annu. Rev. Cell Dev. Biol 2009, 25, 221–251.

[5] Gehart H, Clevers H. Tales from the crypt: New insights into intestinal stem cells. Nat. Rev. Gastroenterol. Hepatol. 2019, 16, 19–34.

[6] Holloway EM, Czerwinski M, Tsai YH, Wu JH, Wu A, Childs CJ, Walton KD, Sweet CW, Yu Q, Glass I, et al. Mapping Development of the Human Intestinal Niche at Single-Cell Resolution. Cell Stem Cell 2021, 28, 568–580.

[7] McCarthy N, Kraiczy J, Shivdasani RA. Cellular and molecular architecture of the intestinal stem cell niche. Nat. Cell Biol. 2020, 22, 1033–1041.

[8] Nomura S, Esumi H, Job C, Tan S-S,1998. Lineage and clonal development of gastric glands. Dev.Biol.204,124–135.

[9] Barker N, Huch M, Kujala P, van de Wetering M, Snippert HJ, van Es JH, Sato T, Stange DE, Begthel H, van den Born M, et al. 2010. Lgr5þve Stem Cells Drive Self-Renewal in the Stomach and Build Long-Lived Gastric Units In Vitro. Cell Stem Cell 6,25–36.

[10] Bjerknes M, Cheng H. Multipotential stem cells in adult mouse gastric epithelium. Am J Physiol – Gastrointest Liver Physiol.2002;283,G767–G777.

[11] Sato T, van Es JH, Snippert HJ, Stange DE, Vries RG, vanden Born M, Barker N, Shroyer NF, vandeWetering M, Clevers H. Paneth cells constitute the niche for Lgr5 stem cells in intestinal crypts. Nature 2011;469,415–418.

[12] Kabiri Z, Greicius G, Madan B, Biechele S, Zhong Z, Zaribafzadeh H, Edison Aliyev J, Wu Y, Bunte R et al. Stroma provides an intestinal stem cell niche in the absence of epithelial Wnts. Development2014;141,2206–2215.

[13] Farin HF, Jordens I, Mosa MH, Basak O, Korving J, Tauriello DVF, dePunder K, Angers S, Peters PJ, Maurice MM, et al. Visualization of a short- range Wnt gradient in the intestinal stem-cell niche. Nature2016;530,340–343.

[14] **Sato T, Vries RG, Snippert HJ, van de Wetering M, Barker N, et al. 2009. Single Lgr5 stem cells build crypt-villus structures in vitro without a mesenchymal niche. Nature 459:262–65**

[15] Sato T, Stange DE, FerranteM,Vries RG, van Es JH, et al. 2011a. Long-term expansion of epithelial organoids from human colon, adenoma, adenocarcinoma, and Barrett's epithelium. Gastroenterology 141:1762–72

[16] Merker SR, Weitz J, Stange DE. Gastrointestinal organoids: How they gut it out. Dev Biol. 2016 Dec 15;420(2):239-250. doi: 10.1016/j.ydbio.2016.08.010. Epub 2016 Aug 10. PMID: 27521455.

[17] Matano, M.,Date,S.,Shimokawa,M.,Takano,A.,Fujii,M.,Ohta,Y.,Watanabe,T., Kanai, T.,Sato,T.(2015).Modeling colorectal cancer using CRISPR-Cas9–mediated engineering of human intestinal organoids. Nat.Med.

[18] Pellegrinet, L.,Rodilla,V.,Liu,Z.,Chen,S.,Koch,U.,Espinosa,L.,Kaestner,K.H., Kopan,R.,Lewis,J.,Radtke,F.(2011).Dll1-andDll4-mediatednotchsignaling are requiredforhomeostasisofintestinalstemcells.Gastroenterology,140, 1230–1240.e7.

[19] Jung P, Sato T, Merlos-Suarez A, Barriga FM, Iglesias M, et al. 2011. Isolation and in vitro expansion of human colonic stem cells. Nat. Med. 17:1225–27

[20] Barker, N.; Huch, M.; Kujala, P.; van de Wetering, M.; Snippert, H.J.; van Es, J.H.; Sato, T.; Stange, D.E.; Begthel, H.; van den Born, M.; et al. Lgr5(+ve) stem cells drive self-renewal in the stomach and build long-lived gastric units in vitro. Cell Stem Cell 2010, 6, 25–36.

[21] McCracken, K.W.; Catá, E.M.; Crawford, C.M.; Sinagoga, K.L.; Schumacher, M.; Rockich, B.E.; Tsai, Y.-H.; Mayhew, C.N.; Spence, J.R.; Zavros, Y.; et al. Modelling human development and disease in pluripotent stem-cell-derived gastric organoids. Nature 2014, 516, 400–404.

[22] Stange,D.E.,Koo,B.-K.,Huch,M.,Sibbel,G.,Basak,O.,Lyubimova,A.,Kujala,P., Bartfeld, S.,Koster,J.,Geahlen,J.H.,etal.,2013.DifferentiatedTroyþ chief cells act asreservestemcellstogeneratealllineagesofthestomachepithelium.Cell 155,357–368.

[23] Schumacher, M.A.,Aihara,E.,Feng,R.,Engevik,A.,Shroyer,N.F.,Ottemann,K.M., Worrell,R.T.,Montrose,M.H.,Shivdasani,R.A.,Zavros,Y.,2015.Theuseof murine-derivedfundicorganoidsinstudiesofgastricphysiology:theuseof fundic organoids.J.Physiol.593,1809–1827

[24] Shin, M, Noji,S., Neubüser,A., Yasugi,S., 2006.FGF10 is required for cell proliferation and gland formationinthestomachepitheliumofthechickenem- bryo. Dev.Biol.294,11–23.

[25] Yui S, Nakamura T, Sato T, Nemoto Y,Mizutani T, et al. 2012. Functional engraftment of colon epithelium expanded in vitro from a single adult Lgr5+ stem cell. *Nat. Med.* 18:618–23

[26] Gjorevski, N. et al. Designer matrices for intestinal stem cell and organoid culture. Nature 539, 560–564 (2016).

[27] Cruz-Acuña, R. et al. Synthetic hydrogels for human intestinal organoid generation and colonic wound repair. Nat. Cell Biol. 19, 1326–1335 (2017).

[28] Calle, E. A. et al. Targeted proteomics effectively quantifies differences between native lung and detergent-decellularized lung extracellular matrices. Acta Biomater. 46, 91–100 (2016).

[29] Gaetani, R. et al. Evaluation of different decellularization protocols on the generation of pancreas-derived hydrogels. Tissue Eng. Part C Methods 24,697–708 (2018).

[30] Dohmen, P. M. Clinical results of implanted tissue engineered heart valves. HSR Proc. Intensive Care Cardiovasc. Anesth. 4, 225–231 (2012).

[31] VeDepo, M. C., Detamore, M. S., Hopkins, R. A. & Converse, G. L. Recellularization of decellularized heart valves: progress toward the tissueengineered heart valve. J. Tissue Eng. 8, 2041731417726327 (2017).

[32] Yu, Y., Alkhawaji, A., Ding, Y. & Mei, J. Decellularized scaffolds in regenerative medicine. Oncotarget 7, 58671–58683 (2016).

[33] Saheli, M. et al. Three-dimensional liver-derived extracellular matrix hydrogel promotes liver organoids function. J. Cell. Biochem. 119, 4320–4333 (2018).

[34] Murphy, S. V., De Coppi, P. & Atala, A. Opportunities and challenges of translational 3D bioprinting. Nat. Biomed. Eng. https://doi.org/10.1038/s41551-019-0471-7 (2019).

[35] VanDussen KL, Marinshaw JM, Shaikh N, Miyoshi H, Moon C, Tarr PI, Ciorba MA, Stappenbeck TS. Development of an enhanced human gastrointestinal epithelial culture system to facilitate patient-based assays. Gut 2015;64:911–920.

[36] Nicholas, W.; Bellono, J.R.; Bayrer, D.B.; Castro, L.J.; Zhang, C.; O'Donnell, T.; Brierley, S.M.; Ingraham, H.A.; Julius, D. Enterochromaffin cells are gut chemosensors that couple to sensory neural pathways. Cell 2017, 170, 185–198.

[37] Middendorp S, Schneeberger K, Wiegerinck CL, Mokry M, Akkerman RD, et al. 2014. Adult stem cells in the small intestine are intrinsically programmed with their location-specific function. *Stem Cells* 32:1083–91

[38] D'Aldebert, E.; Quaranta, M.; Sébert, M.; Bonnet, D.; Kirzin, S.; Portier, G.; Duffas, J.; Chabot, S.; Lluel, P.; Allart, S.; et al. Characterization of Human Colon Organoids From Inflammatory Bowel Disease Patients. Front. Cell Dev. Biol. 2020, 8, 363.

[39] Min, S.; Kim, S.; Cho, S.-W. Gastrointestinal tract modeling using organoids engineered with cellular and microbiota niches. Exp. Mol. Med. 2020, 52, 227–237.

[40] Sayed, I.M.; Sahan, A.Z.; Venkova, T.; Chakraborty, A.; Mukhopadhyay, D.; Bimczok, D.; Beswick, E.J.; Reyes, V.E.; Pinchuk, I.; Sahoo, D.; et al. Helicobacter pylori infection downregulates the DNA glycosylase NEIL2, resulting in increased genome damage and inflammation in gastric epithelial cells. J. Biol. Chem. 2020, 295, 11082–11098

[41] Senger S, Ingano L, Freire R, Anselmo A, Zhu W, Sadreyev R, Walker WA, Fasano A. Human Fetal-Derived Enterospheres Provide Insights on Intestinal Development and a Novel Model to Study Necrotizing Enterocolitis (NEC). Cell Mol Gastroenterol Hepatol. 2018 Jan 31;5(4):549-568. doi: 10.1016/j.jcmgh.2018.01.014.

[42] Li B, Lee C, Cadete M, Miyake H, Lee D, Pierro A. Neonatal intestinal organoids as an ex vivo approach to study early intestinal epithelial disorders. Pediatr Surg Int. 2019 Jan;35(1):3-7. doi: 10.1007/s00383-018-4369-3. Epub 2018 Oct 31. PMID: 30382376

[43] Wu RY, Li B, Koike Y et al (2018) Human milk oligosaccharides increase mucin expression in experimental necrotizing enterocolitis. Mol Nutr Food Res 63:e1800658

[44] Workman MJ, Mahe MM, Trisno S et al (2017) Engineered human pluripotent-stem-cell-derived intestinal tissues with a functional enteric nervous system. Nat Med 23:49–59

[45] Schlieve CR, Fowler KL, Thornton M et al (2017) Neural crest cell implantation restores enteric nervous system function and alters the gastrointestinal

transcriptome in human tissue-engineered small intestine. Stem Cell Rep 9:883–896

[46] Schwank G, Koo B-K, Sasselli V et al (2013) Functional repair of CFTR by CRISPR/Cas9 in intestinal stem cell organoids of cystic fbrosis patients. Cell Stem Cell 13:653–658

[47] Ganousse-Mazeron S, Lacaille F, Colomb-Jung V et al (2015) Assessment and outcome of children with intestinal failure referred for intestinal transplantation. Clin Nutr 34:428–435

[48] Zhang, Y. et al. Excretion of SARS-CoV-2 through faecal specimens. Emerg. Microbes Infect. 9, 2501–2508 (2020).

[49] Lin, L. et al. Gastrointestinal symptoms of 95 cases with SARS-CoV-2 infection. Gut 69, 997–1001 (2020).

[50] Riphagen, S., Gomez, X., Gonzalez-Martinez, C., Wilkinson, N. & Theocharis, P. Hyperinflammatory shock in children during COVID-19 pandemic. Lancet 395, 1607–1608 (2020).

[51] Pique-Regi, R. et al. Does the human placenta express the canonical cell entry mediators for SARS-CoV-2? doi:10.1101/2020.05.18.101485

[52] Bartfeld, S. et al. In vitro expansion of human gastric epithelial stem cells and their responses to bacterial infection. Gastroenterology 148, 126-136.e6 (2015).

[53] Jones, B. C., Calà, G., De Coppi, P. & Giobbe, G. G. Paediatric gastric organoids as a tool for disease modelling and clinical translation. Pediatr. Surg. Int. 1, 3 (2021).

[54] Jung, P. et al. Isolation and in vitro expansion of human colonic stem cells. Nat. Med. 17, 1225–1227 (2011).

[55] Sato, T. et al. Long-term expansion of epithelial organoids from human colon, adenoma, adenocarcinoma, and Barrett's epithelium. Gastroenterology 141, 1762–1772 (2011).

[56] Co, J. Y. et al. Controlling Epithelial Polarity: A Human Enteroid Model for Host-Pathogen Interactions. Cell Rep. 26, 2509-2520.e4 (2019).

[57] Totonelli, G. et al. A rat decellularized small bowel scaffold that preserves villus-crypt architecture for intestinal regeneration. Biomaterials 33, 3401–3410 (2012).

[58] Badylak, StephenF. & Sherry Voytik, G. B. Submucosa gel as a growth substrate for cells. Patent US5866414A (1995).

[59] Voytik-Harbin, S. L., Brightman, A. O., Waisner, B. Z., Robinson, J. P. & Lamar, C. H. Small intestinal submucosa: a tissue-derived extracellular matrix that promotes tissue-specific growth and differentiation of cells in vitro. Tissue Eng.4, 157–174 (1998).

[60] Stokes, D. J. Principles and Practice of Variable Pressure/Environmental Scanning Electron Microscopy (VP-ESEM) (Wiley & Sons, 2008)

[61] **Urciuolo A, Poli I, Brandolino L, Raffa P, Scattolini V, Laterza C, Giobbe GG, Zambaiti E, Selmin G, Magnussen M, Brigo L, De Coppi P, Salmaso S, Giomo M, Elvassore N. Intravital three-dimensional bioprinting. Nat Biomed Eng. 2020 Sep;4(9):901-915. doi: 10.1038/s41551-020-0568-z.**

[62] Wang, M. et al. The trend towards in vivo bioprinting. Int. J. Bioprint. 1, 15–26 (2015).

[63] Drumheller, P. D. & Hubbell, J. A. J. Densely crosslinked polymer networks of poly(ethylene glycol) in trimethylolpropane triacrylate for cell-adhesion-resistant surfaces. Biomed. Mater. Res. 29, 207–215 (1995).

[64] Gjorevski, N. & Lutolf, M. P. Synthesis and characterization of well-defined hydrogel matrices and their application to intestinal stem cell and organoid culture. Nat. Protoc. 12, 2263–2274 (2017).

[65] Manka, S. W. et al. Structural insights into triple-helical collagen cleavage by matrix metalloproteinase 1. Proc. Natl Acad. Sci. USA 109, 12461–12466 (2012).

[66] **Giobbe GG, Crowley C, Luni C, Campinoti S, Khedr M, Kretzschmar K, De Santis MM, Zambaiti E, Michielin F, Meran L, Hu Q, van Son G, Urbani L, Manfredi A, Giomo M, Eaton S, Cacchiarelli D, Li VSW, Clevers H, Bonfanti P, Elvassore N, De Coppi P. Extracellular matrix hydrogel derived from decellularized tissues enables endodermal organoid culture. Nat Commun. 2019 Dec 11;10(1):5658. doi: 10.1038/s41467-019-13605-4.**

[67] Zhang, H. et al. Digestive system is a potential route of COVID-19: An analysis of single-cell co-expression pattern of key proteins in viral entry process. Gut 69, 1010–1018 (2020).

[68] C. Frantz, K.M. Stewart, V.M. Weaver, The extracellular matrix at a glance, J. Cell Sci. 123 (2010) 4195–4200, https://doi.org/10.1242/jcs.023820

[69] K.A. Moore, I.R. Lemischka, Stem cells and their niches, Science 80 (2006) 1880–1885, https://doi.org/10.1017/CBO9780511997839.006, 311.

[70] A.J. Engler, S. Sen, H.L. Sweeney, D.E. Discher, Matrix elasticity directs stem cell lineage specification, Cell 126 (2006) 677–689, https://doi.org/10.1016/j.cell.2006.06.044.

[71] Tibbitt, M. W. & Anseth, K. S. Hydrogels as extracellular matrix mimics for 3D cell culture. Biotechnol. Bioeng. 103, 655–663 (2009).

[72] Sato, T. et al. Single Lgr5 stem cells build crypt-villus structures in vitro without a mesenchymal niche. Nature 459, 262–265 (2009).

[73] Cruz-Acuña, R. et al. Synthetic hydrogels for human intestinal organoid generation and colonic wound repair. Nat. Cell Biol. 19, 1326–1335 (2017).

[74] Nelson, C. M. & Bissell, M. J. Of extracellular matrix, scaffolds, and signaling: tissue architecture regulates development, homeostasis, and cancer. Annu. Rev. Cell Dev. Biol. 22, 287–309 (2006).

[75] Gjorevski, N. et al. Designer matrices for intestinal stem cell and organoid culture. Nature 539, 560–564 (2016).

[76] Simo, P. et al. Changes in the expression of laminin during intestinal development. Development 112, 477–487 (1991)

[77] Lamers, M. M. *et al.* SARS-CoV-2 productively infects human gut enterocytes. *Science (80-.).* **369**, 50–54 (2020).

[78] Zhou, J. et al. Infection of bat and human intestinal organoids by SARS-CoV-2. Nat. Med. 1–7;(2020). doi:10.1038/s41591-020-0912-6

[79] Lamers, M. M. et al. SARS-CoV-2 productively infects human gut enterocytes. Science (80-.). 369, 50–54 (2020).

[80] Tian, Y., Rong, L., Nian, W. & He, Y. Review article: gastrointestinal features in COVID-19 and the possibility of faecal transmission. Aliment. Pharmacol. Ther. 51, 843–851 (2020).

[81] **Giobbe GG, Bonfante F, Jones BC, Gagliano O, Luni C, Zambaiti E, Perin S, Laterza C, Busslinger G, Stuart H, Pagliari M, Bortolami A, Mazzetto E, Manfredi A, Colantuono C, Di Filippo L, Pellegata AF, Panzarin V, Thapar N, Li VSW, Eaton S, Cacchiarelli D, Clevers H, Elvassore N, De Coppi P. SARS-CoV-2 infection and replication in human gastric organoids. Nat Commun. 2021 Nov 16;12(1):6610. doi: 10.1038/s41467-021-26762-2.**